An Ultrafast Source of Polarization Entangled Photon Pairs based on a Sagnac Interferometer

by

Devin Hugh Smith

A thesis
presented to the University of Waterloo
in fulfillment of the
thesis requirement for the degree of
Master of Science
in
Physics

Waterloo, Ontario, Canada, 2009

Abstract

This thesis describes the design, development, and implementation of a pulsed source of polarization-entangled photons using spontaneous parametric down-conversion in a Sagnac interferometer. A tangle of 0.9286 ± 0.0015, fidelity to the state $(|10\rangle + |01\rangle)/\sqrt{2}$ of 0.9798 ± 0.0004 and a brightness of 597 pairs/s/mW were demonstrated.

Spontaneous parametric down-conversion is a nonlinear optical process in which one photon is split into two lower-frequency photons while conserving momentum and energy, in this experiment nearly degenerate photons are produced. These photons are then interfered at the output beamsplitter of the interferometer, exchanging path entanglement for polarization entanglement and generating the desired polarization-entangled photon pairs.

Acknowledgements

For his support and advice during the entire process of my degree, from novice grad student to graduand, I must first thank my advisor Gregor Weihs: without him none of this research is possible. I must also thank the members of the photonic entanglement group, especially Rainer Kaltenbaek and Christophe Couteau, for advice and discussion regarding both my work and otherwise. I must further thank Immo Söllner for keeping the lab relaxed and Chris Erven for the use of some of his computer code.

On a more personal level, I would like to thank my friends and family for their love and encouragement. My mother, Anna Veldhuis, deserves most of the credit for making me who I am today, and without her I would not be writing this thesis. Bill Rosgen, the best friend I have made since starting this degree, deserves thanks for keeping me sane, and exposing me to the theoretical side of quantum computing. Jen Fung has kept me sane and alive during the final days of my degree, from the final experiments through to the submission of my thesis, and also deserves credit for being my primary proofreader.

My girlfriend, Holly Lay, recieves my most heartfelt thanks, however. For supporting me as I moved four hours up the road for more than two years to do this degree, for her love and support, for her presence in my life, and for all the other things she does for me, big and small, thanks go to her.

Contents

List of Tables

List of Figures

Chapter 1

Introduction

1.1 Motivation

Quantum optics, as a field, is always in need of brighter and higher quality sources of quantum light, new and more efficient photon detectors, and, perhaps, some experiments to place in between. In this thesis, I am dealing with the first of these topics: the creation of an ultrafast entangled photon pair source. To a layperson, the problem of creating a single photon seems trivial; however, this is not the case. Currently, two choices appear to be available to us: stochastic techniques based almost entirely on spontaneous parametric down-conversion, which generates two mode squeezed states that can be approximated as two single photon states; and deterministic schemes based on the excitation of a physical system which have a very low success probability. I will speak no more of the latter in this thesis, as they lie outside the scope of it.

There are many criteria for the evaluation of photon pair sources: the brightness, or number of photon pairs created; the spectral brightness, or number of photon pairs created in a given bandwidth; the fidelity, or the degree to which the desired state was created; and the tangle, a measure of the entanglement of the state, for example. There are also many applications with diverse requirements: entanglement-based quantum cryptography requires exactly two photons at a time, and is aided by a high repetition rate; while cluster-state quantum computing requires the generation of many photons at once. Even a relatively simple experiment such as entanglement swapping between two photon pairs has certain requirements: two independently generated and yet indistinguishable photon pairs must arrive at a beamsplitter at the same time.

In 2006, Kim, Fiorentino and Wong [1] published a paper reporting a new and exciting kind of photon pair source based on a Sagnac interferometer. Instead of generating many photons and rejecting all but those that are entangled, occupying a small angle, they set up a system that entangled all of the photons that could be collected, allowing a greater number of usable pairs to be generated. This was accomplished by generating the photons inside an interferometer, hiding the information about which path was used to create the photons.

This sort of scheme had been tried before, with varying results, but the breakthrough idea of this implementation was the use of a Sagnac interferometer [2]. This type of interferometer is a loop about which light travels in both directions, using the same optics for both beam paths. The primary use of these interferometers in classical physics is to measure the speed at which the interferometer is spun: the light picks up a phase to

$$\frac{4\vec{\omega} \cdot \vec{A}}{c\lambda}, \tag{1.1}$$

the rotation speed times the area over the speed of light times the wavelength, which was used, for instance, to make the first measurement of the absolute rotation speed of the earth [3]. Currently, the same effect is used in laser gyroscopes, which are found in every commercial aircraft.

However, for the purposes to which quantum optics puts it, the primary virtue of the Sagnac interferometer is its stability and predictability: due to the use of all of the same optics for the interfering beams it is phase stable, and as there are no tunable phases inside the interferometer the outputs need not be tuned. One simply places a crystal designed to emit photon pairs collinear to a pump beam in an interferometer loop, and an efficient photon pair source is created.

The initial paper by Kim, Fiorentino and Wong [1] initiated a flurry of similar research in other research groups, complementing continued research in their group [4]: conventional Sagnac source programs are in place in Vienna [5] and Brisbane [6], while derivative systems are being developed in Bristol and Toronto [7], amongst other places. My project is part of this collection of new research directions.

Effectively, there are two categories of photon pair sources: continuous wave (CW) sources, typically used for experiments that require only one pair of photons, such as quantum key distribution; and pulsed sources designed for experiments requiring more than one photon pair. As SPDC is a fast process, the additional timing constraint provided by the short pulses of an ultrafast laser allows the outputs of several photon sources to be interfered, as we can ensure that the outputs of both photon sources arrive at nearly the same time.

The first generation of Sagnac-type sources were CW, as they are both cheaper and easier to build. The obvious extension of such work was to attempt the same or similar design while operating the source with a fast laser—this idea is the genesis of my project.

A secondary goal of this project was to reduce costs: this manifested itself in a design decision to change from a single interferometric loop to a dual interferometer design, discussed later, as well as an attempt to reduce the cost of various components such as free-space-to-fibre couplers.

1.2 Definitions

1.2.1 Pure and Mixed States

The state of a photon has many degrees of freedom of which some have a continuous spectrum, such as frequency. However, for the purposes of this thesis, I will be treating each photon as a two-level system in some mode $\vec{k}$, that carries one bit of information encoded in its polarization, except when it becomes necessary to be concerned with other degrees of freedom. These form a basis for a Hilbert space, $\mathfrak{H}$, encoded by

$$|H\rangle \mapsto |0\rangle \equiv \begin{bmatrix} 1 \\ 0 \end{bmatrix} \tag{1.2}$$

$$\text{and}\, |V\rangle \mapsto |1\rangle \equiv \begin{bmatrix} 0 \\ 1 \end{bmatrix}, \tag{1.3}$$

where $|H\rangle$ and $|V\rangle$ represent a photon in a horizontally or vertically polarized state, respectively. All fully polarized states of a photon can be expressed as combinations of these states; for instance, circularly polarized light is given by $(|0\rangle \pm i|1\rangle)/\sqrt{2}$, where the handedness is determined by convention. In this thesis, I will assign $(|0\rangle + i|1\rangle)/\sqrt{2}$ to right circular polarization.

However, not all states are maximally polarized; in the formalism of quantum mechanics, these are known as mixed states, which represent probabilistic mixtures of quantum states. In order to treat these states mathematically we must leave the state-vector formalism and treat states as matrices. The density matrix, ρ, of some pure state $|\psi\rangle$ is

$$\rho := |\psi\rangle \langle\psi|, \tag{1.4}$$

with mixtures of states given by combinations thereof. If we have some collection of states $|\psi_j\rangle$ each with probability p_j, then the density matrix of the mixture is

$$\rho := \sum_j p_j |\psi_j\rangle \langle\psi_j|. \tag{1.5}$$

An unpolarized beam of single photons is an equal mixture of all polarizations of light, and thus is represented by $\rho = \mathbb{I}_2/2$, the identity matrix in two dimensions. Some useful properties of density matrices are as follows:

- $\mathrm{Tr}(\rho) = 1$;
- $\rho \geqslant 0$, that is, ρ is positive semi-definite;
- $\rho = \tau\tau^\dagger$ for some upper triangular matrix τ, where † represents the conjugate transpose;
- ρ is Hermitian.

A two-photon state exists in a Hilbert space formed by the combination of their individual spaces, $\mathfrak{H}_a \otimes \mathfrak{H}_b$, leading to a basis formed by $|00\rangle$, $|01\rangle$, $|10\rangle$, and $|11\rangle$, where the first character is the state of the first photon and the second that of the second photon. Thus, these four basis states are simply all of the combinations of the possible basis states of the two photons.

1.2.2 Projective Measurements

Unfortunately, the standard formalism for measurements in quantum mechanics, the projective measurement, is not accurately reflected in the reality of most quantum optics experiments. In this formalism, one simply chooses a basis for measurement. The quantum state is projected onto one of the basis elements with probability given by the overlap squared and the measurement device outputs classical information indicating onto which state the input was projected.

This is not how my experiment, nor most of those in quantum optics, works: only one state can be measured at a time, and after measurement the state is demolished, not simply projected onto the basis state in question. We can build a projector onto an arbitrary polarization state simply, using a quarter waveplate and a linear polarizer, this provides our measurement device: all states not projected onto this projector are simply rejected. One could conceive of using a polarizing beamsplitter to allow for the detection of two orthogonal states, however this adds significant complexity to the measurement apparatus, as an additional fibre coupler is required; furthermore, the reflected arm of a PBS is much poorer than the transmitted arm.

The measurement, then, is a simple binary output. The input density matrix ρ is measured to be in the state $|\phi\rangle$, chosen by the experimenter, with probability $\mathrm{Tr}(\rho\,|\phi\rangle\langle\phi|)$; otherwise, no state is received. This is the "click–no-click" detection scheme: if multiple photons are present, and any of them pass the polarizer then the detector clicks, thus all the information we get is that *at least* one photon has been detected.

One further important detail is the significant imperfection of measurements as performed in the lab. The most obvious imperfection in the system is that even a perfect state will be detected much less than 100% of the time even if $\rho = |\phi\rangle\langle\phi|$, as there are many inefficiencies in the system: at best we can expect about a 35% success rate (see 3.5).

1.2.3 Fidelity

The fidelity, $\mathcal{F}(\rho, \sigma)$, of two quantum states is the measure of how close they are together. For pure states it is simply the overlap of those two quantum states, thus:[1]

$$\mathcal{F}\left(|\phi\rangle\langle\phi|, |\psi\rangle\langle\psi|\right) = |\langle\phi|\psi\rangle| \,. \tag{1.6}$$

For mixed quantum states the most convenient definition of the fidelity, in easily calculable terms, is given by [8]

$$\mathcal{F}(\rho, \sigma) = \mathrm{Tr}\left(\sqrt{\sqrt{\rho}\,\sigma\sqrt{\rho}}\right), \tag{1.7}$$

which, by the cyclic property of the trace[2], easily reduces to equation 1.6 when ρ and $\sigma = |\psi\rangle\langle\psi|$ are pure states. Several useful properties of the fidelity are:

- $\mathcal{F}(\rho, \rho) = 1$;
- $\mathcal{F}(\rho, \sigma) = \mathcal{F}(\sigma, \rho)$;
- $0 \leqslant \mathcal{F}(\rho, \sigma) \leqslant 1$;
- $\mathcal{F}(\rho, \sigma) = 1 \Rightarrow \rho = \sigma$.

The fidelity between the goal state and that produced can be a measure of success of the experimental production of a desired state, and this is how I shall be using it.

---

[1] Some physicists define the fidelity as the overlap squared. Care should be taken to note the convention in use in a given publication.

[2] $\mathrm{Tr}(abc) = \mathrm{Tr}(bca) = \mathrm{Tr}(cab)$

1.2.4 Interferometric Visibility

When examining an interference pattern, the visibility, V, of the fringes of the pattern is a good measure of the quality of the interference. This is defined simply as

$$V = \frac{I_{\text{max}} - I_{\text{min}}}{I_{\text{max}} + I_{\text{min}}}\,, \tag{1.8}$$

where the Is are intensities of light taken at extrema of the interference pattern.

Of course, such an idea can also be applied to quantum states measured as a function of the angle of measurement. Consider the singlet state $(|01\rangle - |10\rangle)/\sqrt{2}$: if we project the first qubit on the state $|0\rangle$, and the second qubit is projected upon the state $\sin\theta|0\rangle + \cos\theta|1\rangle$ by rotating a polarizer through an angle θ, then the probability of getting a click is proportional to $\sin^2(\theta)$.

This is equivalent to interference fringes, and so the same definition can apply simply substituting photon count rates for intensities:

$$V = \frac{N_{\text{max}} - N_{\text{min}}}{N_{\text{max}} + N_{\text{min}}}\,. \tag{1.9}$$

However, count rates can vary depending on the settings of the various optics, independent of the quality of the states produced, due to slightly wedged or misaligned optics. To take this into account, it is best to unbias the measurement of visibility. If we are looking at the visibility in the basis defined by $|a\rangle$ and $|b\rangle$[3], this unbiased visibility is given by:

$$V = \pm\frac{N_{aa} + N_{bb} - N_{ab} - N_{ba}}{N_{aa} + N_{bb} + N_{ab} + N_{ba}}\,, \tag{1.10}$$

with the sign chosen to make V positive: the parity depends upon the symmetry of the chosen state. Note that this is simply the visibility averaged over the interchange of the first and second photons.

1.2.5 Tangle

An entanglement monotone, E, is a measure of the degree of entanglement of a system. An entanglement monotone is 0 for all separable states, 1 for all maximally entangled states, and non-increasing with local operations on the parts of the system and classical communication between them.

There are many choices of entanglement measures for different contexts, as discussed in a review by the Horodeckis [9]. However, recently, the most popular measure for two-qubit entanglement in quantum optics has been the tangle, as defined in Coffman, Kundu and Wooters' paper[4] [10]. This is simply the concurrence squared, while the concurrence is defined in a slightly complicated way: let

$$\Sigma = \sigma_y^{\otimes 2} = \begin{bmatrix} 0 & 0 & 0 & -1 \\ 0 & 0 & 1 & 0 \\ 0 & 1 & 0 & 0 \\ -1 & 0 & 0 & 0 \end{bmatrix} \tag{1.11}$$

---

[3] $\langle a|b\rangle = 0$

[4] Note that in the reference given the 'squared concurrence' is the first appearance of tangle in a publication. The term 'tangle' appeared in the preprint and in later literature, but was removed for publication at the request of the journal.

be the spin-flip matrix for two qubits. Then let

$$\tilde{\rho} = \Sigma \, \rho \, \Sigma \tag{1.12}$$

and

$$R = \sqrt{\sqrt{\rho} \, \tilde{\rho} \sqrt{\rho}} \, . \tag{1.13}$$

Then the concurrence, $\mathcal{C}$, is given by

$$\mathcal{C} = \max \left\{ 0, \sqrt{R_1} - \sqrt{R_2} - \sqrt{R_3} - \sqrt{R_4} \right\} \tag{1.14}$$

where the R_j are the eigenvalues of R in decreasing order[5].

The initial interest in the concurrence stemmed from its connexion to the entanglement of formation, $\mathcal{E}$, which is given by

$$\mathcal{E}(\mathcal{C}(\rho)) := h \left(\frac{1 + \sqrt{1 + \mathcal{C}^2}}{2} \right) \tag{1.15}$$

where

$$h(x) := -x \log_2 x - (1 - x) \log_2 (1 - x). \tag{1.16}$$

It so happens that the tangle, $T := \mathcal{C}^2$, has several useful additive properties when dealing with multipartite entanglement; the strongest of these is

$$T(A, B) + T(A, C) \leqslant T(A, BC) \, . \tag{1.17}$$

It is unclear to me why the tangle has become the preferred entanglement measure for biphotonic states (as opposed to, say, the entanglement of formation or the concurrence), but it has become nearly universal and thus it will be used herein to compare my results to each other as well as to those found in the literature.

1.3 Quantum State Tomography

The problem of deciding if the quantum state one set out to create has actually been created turns out to be nontrivial. The obvious goal, to determine the density matrix for the quantum state generated by an experiment, is algorithmically hard to accomplish, requiring $O(4^n)$ time[6]. Fortunately, only the case where the quantum state-space is four-dimensional (*i.e.* a two qubit system) is of interest to me, which is feasible to compute.

Nathan Langford's thesis [12] contains an extensive discussion of quantum state tomography in optics, and is recommended reading for those wishing to explore the subject

---

[5] This seemingly complicated definition arises from the definition of the concurrence in the special case of pure states. For a pure state $|\psi\rangle$, the concurrence is defined as $|\langle\psi| \, \Sigma \, |\psi\rangle|$, where Σ is a spin-flip matrix of appropriate dimension. It turns out that the definition given above is the correct extension of the concurrence to mixed states of two qubits[11], such that, for instance, the entanglement of formation can be calculated in the same way.

[6] This is the best known algorithm for the problem: as in all problems in complexity theory, a good lower bound is unavailable. Note that this assumes that n qubit states are available on demand: for a stochastic system like those used in quantum optics it is worse by another exponential factor.

in detail. Here, I will give a more concise summary of the process of state tomography sufficient to allow for the interpretation of the results of this thesis.

Due to Heisenberg's uncertainty principle, measuring one instance of a quantum state is insufficient to determine its quantum state exactly with certainty: we must therefore prepare an ensemble of identical quantum states and perform sufficient measurements to statistically determine the quantum state. Of course, this assumes that our state production process is perfectly repeatable; any lack of repeatability will lead to a mixture of quantum states in our measurement.

We have, for a two qubit system, $2^{2^2} = 16$ free parameters to determine a density matrix. The requirement that the state be normalized would provide an additional constraint, except that probabilities are not measured; instead, count rates are measured, and these must be normalized, reintroducing that degree of freedom.

These sixteen parameters represent a basis for the density matrices, say

$$\rho = \sum_{j=1}^{16} v_j V_j, \tag{1.18}$$

where the V_j are basis operators and the v_j are the real parameters needed. The V_j can be chosen to be orthogonal, *i.e.* $\mathrm{Tr}(V_j V_k) = \delta_{jk}$. Unfortunately, there are only four orthogonal projectors in a two qubit system, so the orthogonal basis V_j can not be constructed out of projectors. As projective measurements are far simpler to construct in the lab than positive operator valued measurements[7], a second, nonorthogonal basis for the 4-by-4 density matrices must be constructed. Any set of 16 linearly independent projectors will do, though the tetrahedral projectors are the optimal minimum set: these consist of projection onto all combinations of $|0\rangle$, $\frac{1}{2}|0\rangle + \frac{\sqrt{3}}{2}|1\rangle$, $\frac{1-\sqrt{3}i}{4}|0\rangle + \frac{3i+\sqrt{3}}{4}|1\rangle$, and $\frac{1+\sqrt{3}i}{4}|0\rangle + \frac{3i+\sqrt{3}}{4}|1\rangle$ for each of the qubits. Note that this set of projectors is invertible to give the V_j in terms of them, yielding the process known as linear state tomography; however, due to experimental noise this often yields an unphysical density matrix.

Maximum likelihood tomography solves this problem, and can be performed with a minimal set of projectors, but as shown by Langford [12] using an over-complete set of measurements is both more accurate for a given total measurement time and simpler to implement. The set of projectors

$$W_j = (\{\{|0\rangle, |1\rangle\}, \{|\pm\rangle = |0\rangle \pm |1\rangle\}, \{|\pm i\rangle = |0\rangle \pm i|1\rangle\}\})^{\otimes 2} \tag{1.19}$$

is a natural, easy-to-implement set of measurements where each subset forms a complete projective measurement, which allows them to be normalized separately: this requires six measurements for each of the two qubits instead of four: 36 total measurements instead of sixteen. A measurement is taken of each of the projectors W_j on some ensemble of qubits sufficient to reach a good estimate of the true value of $\mathfrak{W}_j/\mathfrak{N}$, assuming Poissonian noise, where $\mathfrak{W}_j$ is the number of qubits that were projected onto W_j, and $\mathfrak{N}$ is a normalization parameter.

1.3.1 Maximum Likelihood Tomography

Having taken this set of 36 measurements, the reconstruction of the density matrix, ρ, can commence. The goal is to find the density matrix, ϱ, most likely to correspond to

---

[7] Positive operator valued measures are the generalisation of projective measurements wherein several of the restrictions on the measurement are relaxed. I will not be discussing them further in this thesis.

the set of measurements taken: the following method is due to James *et al.*[13].

The process is effectively the same procedure as used in least-squares fitting: a penalty function, ϖ, is minimized with respect to the input parameters such that the estimated density matrix, ϱ, is most likely to have been that generating the data measured given the noise sources present in the experiment.

One possible parametrization of a density matrix, ρ, into orthogonal parameters V is suggested by one of the properties listed in section 1.2.1: $\rho = \tau\tau^\dagger$ for some upper triangular matrix, τ, with a real diagonal. Our sixteen real parameters are then the components of the matrix:

$$\tau = \begin{bmatrix} t_1 & t_2 + it_3 & t_4 + it_5 & t_6 + it_7 \\ 0 & t_8 & t_9 + it_{10} & t_{11} + it_{12} \\ 0 & 0 & t_{13} & t_{14} + it_{15} \\ 0 & 0 & 0 & t_{16} \end{bmatrix} \tag{1.20}$$

Then the penalty function used is the distance in quadrature between the current prediction for each measurement, $w_j(\varrho) = \mathrm{Tr}(\varrho W_j)$, and our measurements $\mathfrak{W}_j$. That is:

$$\varpi(t) := \sum_{j=1}^{36} \frac{(\mathfrak{W}_j - w_j(t))^2}{\mathfrak{W}_j} \tag{1.21}$$

where each measurement is weighted by its error. Note that the choice to use the measured counts, $\mathfrak{W}_j$, as the error weights, and not the number of counts predicted from the fit, $w_j(\rho)$, is somewhat arbitrary; Monte Carlo simulations show that the $\mathfrak{W}_j$ provide somewhat better results, and is also computationally simpler to implement. This penalty function, $\varpi(t)$, assumes that each of the $\mathfrak{W}_j$ is collected individually as described in section 1.2.2—if the projective measurements are complete, then the noise only applies to the total count for the measurement.

The normalization of ϱ is uncontrolled by this procedure: the inputs, $\mathfrak{W}_j$, are counts, not probabilities, but this is simple to correct by dividing through by $\mathfrak{N} = \mathrm{Tr}\,\varrho$; moreover, allowing the normalization to be unconstrained during the minimization procedure allows $\mathfrak{N}$ to be determined by all of the measurements, not simply those in the computational basis.

However, I am neglecting one of the more compelling reasons to use over-complete tomography: each subset of four projectors forms a complete measurement, allowing for the normalization of each of these subsets before the maximum likelihood optimization is performed. This reduces the effect of variable coupling efficiency for different projective measurements on the system, and also reduces the effects of drift on the results as the system need only be stable for four measurements, instead of the full 36.

Therefore, before performing the maximum likelihood reconstruction $\mathfrak{W}_j$ is divided by the sum of members of the same measurement set; for instance if $\mathfrak{W}_n$ is the projector $|0\rangle\langle 0| \otimes |+\rangle\langle +|$ then the other members of this projective measurement set are $\{|1\rangle\langle 1| \otimes |+\rangle\langle +|, |1\rangle\langle 1| \otimes |-\rangle\langle -|, |0\rangle\langle 0| \otimes |-\rangle\langle -|\}$. This processing provides a more accurate value to put in the numerator of $\varpi(t)$: the denominator, however, remains as $\mathfrak{W}_j$ since this is linearly proportional to the noise on the normalized $\mathfrak{W}_j$.

1.3.2 Monte Carlo Simulation of Errors

Any experiment has only finite accuracy, and an experimentalist must report that accuracy along with his results. Maximum likelihood tomography, however, does not admit an analytical solution to the estimation of the accuracy of the proecedure, nor, more fatally, to the estimation of the uncertainty in the derived parameters due to experimental uncertainties; the standard approach used in the literature has been to estimate them via Monte Carlo techniques. These techniques allow us to simulate the experiment as performed a number of times to find an estimate of the experimental uncertainties involved, without the difficulty of actually repeating the experiment hundreds of times.

For each for the $\mathfrak{W}_j$, a normally-distributed estimate with standard deviation $\sqrt{\mathfrak{W}_j}$ is chosen at pseudo-random[8]. Note that the Gaussian distribution is centred at the sample point and not the actual value; this is unavoidable in experiments.

Having chosen an array of $\mathfrak{W}_j$, it is a simple matter to run the maximum likelihood method again to come up with a new estimated density matrix. Repeating this process a sufficient number of times an estimate of the errors in a given result can be obtained: either for the elements of the density matrix directly, or for derived items. It has been shown via Monte Carlo simulation [12] that 200 samples are sufficient to for it to be likely that the standard error has converged to one significant digit, the usual reporting standard.

It was not clear to me, however, that this approach fully characterizes the errors possible in these calculations. A primary source of error, the misalignment of the polarization analyser for each state, is completely neglected by this method. A random deviation of each projector could be made to account for this, but this is made difficult due to correlated errors: the measurement order for state tomography is typically chosen to minimize the number of optics rotated between each step, leading to partly correlated errors in the measurements taken. For sufficiently high count numbers, this source of error will dominate the shot noise of counting statistics.

Furthermore, in high-quality photon sources the states produced are close to maximally entangled and pure, and an examination of the histograms produced by the Monte Carlo method shows significant asymmetry in the distribution, depending on the state chosen. To examine this further, I ran 30 000 simulations for one of my measured sets of data and calculated the tangle for each one. The histogram is shown in figure 1.1, and is clearly asymmetric, with a skewness of -0.0053: for higher quality states the effect should be even higher. Care must be taken in the reporting of errors for experiments of this type to ensure that it is reported correctly, *i.e.* simply reporting the standard deviation of the data may be insufficient. I will report all errors to a 95% confidence interval and report different errors if necessary for the positive and negative errors.

1.4 Spontaneous Parametric Down-Conversion

Spontaneous parametric down-conversion (SPDC) is a second-order nonlinear optical process in which one pump photon is converted into two lower frequency photons, tradition-

---

[8] Each of the counts, $\mathfrak{W}_j$, suffers from Poissonian noise, and are generally sufficiently large that $\mathfrak{W}_j \gg \sqrt{\mathfrak{W}_j}$, thus treating the error as Gaussian is a good approximation. For very small (or zero) measured values of $\mathfrak{W}_j$, greater care must be taken to treat the noise exactly.

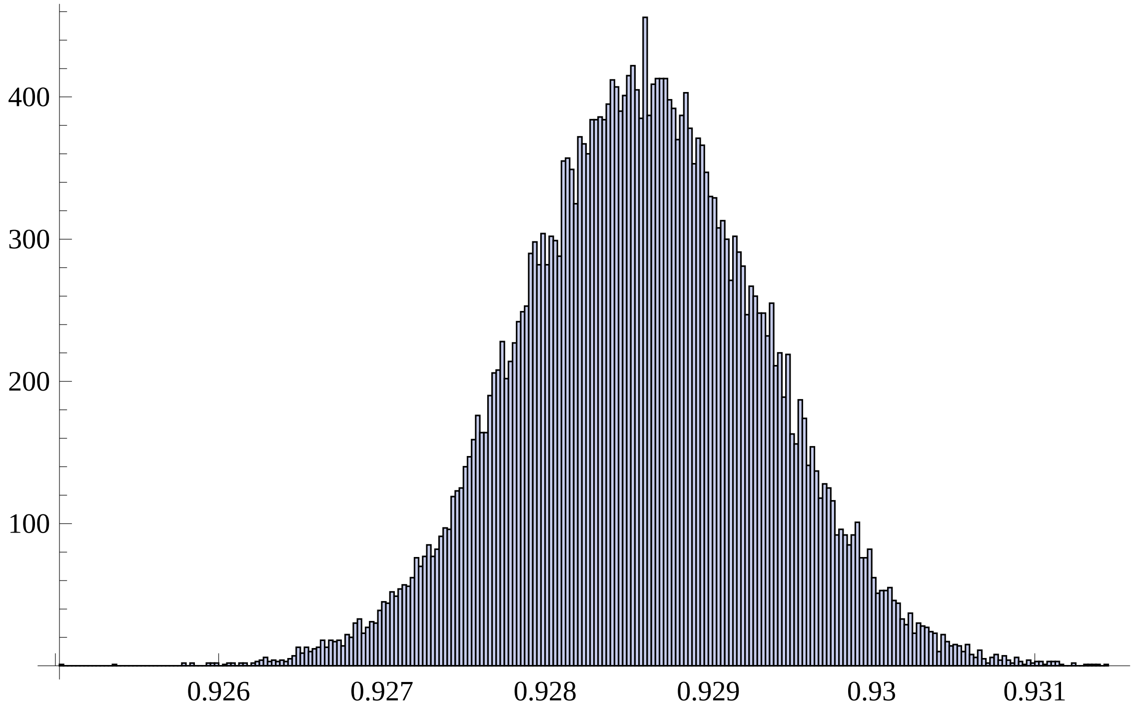

Figure 1.1: A histogram showing counts v. tangle for 30 000 iterations of a Monte Carlo simulation. Note that the curve is not symmetric: the tail to the right is longer than that to the left, leading to a difference in 2σ reported error of 4%.

ally known as the *signal* and the *idler*, in a process that conserves momentum and energy,

$$\vec{k_p} = \vec{k_s} + \vec{k_i} \quad \& \tag{1.22}$$

$$\omega_p = \omega_s + \omega_i \,, \tag{1.23}$$

where $\vec{k}$ is momentum, ω is the frequency, and subscripts p, s, and i refer to the pump, signal, and idler photons, respectively. A very good introduction to the topic is given by Marek Żukowski in his lecture notes [14].

The likelihood of SPDC is controlled by the $\chi^{(2)}$ nonlinear tensor, as all three-photon nonlinear processes are: $\chi^{(2)}$ is a function of material, wavelengths, temperature, and crystal structure. The interaction Hamiltonian for second order nonlinear optical processes is[9]:

$$H = \varepsilon_0 \int_V \mathrm{d}^3 r \, \chi_{\hat{k}_p \hat{k}_s \hat{k}_i} E_p^+ E_s^- E_i^- + \text{H.C.} \tag{1.24}$$

where V is the volume illuminated by the pump beam, H.C. is the Hermitian conjugate, E_s and E_i are given by

$$E_{s,i}^+ = \sum_{\vec{k}} \vec{E}_{\vec{p}\vec{k}} a_{\vec{p}\vec{k}} e^{i(\vec{k}\cdot\vec{r} - \omega_{\vec{p}\vec{k}} t)} \,, \tag{1.25}$$

where $\vec{p}$ is the polarization vector and E_p is a monochromatic classical field, given by

$$E_p = \vec{E_0} e^{i(\vec{k}\cdot\vec{x} - \omega t - \phi)} + \text{c.c.} \tag{1.26}$$

---

[9] I will hereafter drop the superscript on $\chi^{(2)}$ at times for clarity

where c.c. is the complex conjugate. The extension from monochromatic plane waves to combinations of wavelengths is straightforward: as pulses get very short the momentum-matching condition is relaxed.

The two-photon state produced is

$$|\psi_{\mathrm{SPDC}}\rangle = \int \mathrm{d}\omega_p \, g(\omega_p) e^{i\omega_p \tau_p} \iint \mathrm{d}\omega_s \; \mathrm{d}\omega_i \, \delta(\omega_p - \omega_s - \omega_i) \hat{a}_1^\dagger(\omega_s) \hat{a}_2^\dagger(\omega_i) \, | \quad \rangle \, , \tag{1.27}$$

where $\hat{a}_1^\dagger$ and $\hat{a}_2^\dagger$ are the creation operators into two distinct modes, $g(\omega_p)$ is the distribution of wavelengths in the pump beam, τ_p is the arrival time of the pump, and $| \quad \rangle$ is the vacuum. Here I have made the nondepleted pump approximation, *i.e.* that the pump is a strong classical field that is not affected by the SPDC process, and as SPDC in free space is not more than 10^{-8} efficient this is not a strong assumption.

1.4.1 Quasi-phase-matching

Fortunately, it is possible to relax the phase-matching conditions slightly by engineering of the non-linear crystal used. The example I will discuss here is periodic poling; however, others also exist. $\chi^{(2)}$ is a tensor that requires a lack of inversion symmetry in a crystal, which has some important consequences. The one that is immediately useful is

$$\chi_{i,j,k} = -\chi_{-i,-j,-k} = -\chi_{-i,j,k} \, . \tag{1.28}$$

Thus, if the crystallographic axes are reversed, then the relative phase is shifted by π. If a grating along the propagation direction is built, which reverses the crystal structure periodically, then this effectively introduces an additional momentum vector into the momentum-matching condition:

$$\vec{k}_p = \vec{k}_s + \vec{k}_i + \vec{G} \tag{1.29}$$

where $\vec{G}$ is an odd multiple or divisor of the grating period. Typically, $\vec{G}$ is chosen to be the first-order reciprocal lattice vector for ease of construction as well as conversion efficiency, but fabrication concerns may require a longer grating to be made.

One surprising consequence of this scheme is that while this quasi-phase-matching is of lower efficiency than perfect phase-matching, it is only less efficient by a constant factor: for first order quasi-phase-matching it is so by $2/\pi$ as compared to for an otherwise identical crystal[15]. It does, however, allow us to choose a propagation direction that maximizes χ_{ijk}, and eliminate lateral walk-off by propagating all three beams directly along one of the crystallographic axes and aligning the polarization directions along the remaining two.

For my purposes, I require collinear outputs from SPDC: both the signal and idler photons emitted into the same spatial mode. Then the state is given by

$$|\psi\rangle = \iint \mathrm{d}\omega_s \, \mathrm{d}\omega_i \, g(\omega_s + \omega_i) e^{i(\omega_s + \omega_i)\tau_p} \hat{a}_V^\dagger(\omega_s) \hat{a}_H^\dagger(\omega_i) \tag{1.30}$$

where the creation operators, a, are assumed to have the same $\vec{k}$, and a polarization specified by the subscript.

The end result is a two mode squeezed state, which can be approximated by

$$|\psi(t)\rangle \propto |\quad\rangle + p a_H^\dagger a_V^\dagger |\quad\rangle + p^2 a_H^{\dagger 2} a_V^{\dagger 2} |\quad\rangle + O(p^3) \tag{1.31}$$

where p is the probability of getting a photon pair at some time[10] t: for low values of p the six-fold and higher photon contributions become negligible.

1.4.2 Rate of Spontaneous Parametric Down-Conversion

Recent work by Ling, Lamas-Linares, and Kurtsiefer [16] on the absolute rate of down-conversion provides an estimate and upper bound on the number of photons produced. In the collinear case, the rate of photons emitted into the output modes, across all spectral frequencies, $\tilde{R}_T$, is given by

$$\frac{\tilde{R}_T}{Pl} \lessapprox \frac{4d^2\omega_p^2}{9\pi\varepsilon_0 c^2 n_s n_i n_p |n_i - n_s| W_p^2} \tag{1.32}$$

where d is the relevant contraction of $\chi^{(2)}$ given the polarization and propagation vectors of the three beams, in my case 2.8 pm/V, W_p the pump beam waist, ϵ_0 the permittivity of free space, c the speed of light in vacuum, P the total pump power, and l the crystal length. For the beam parameters present in our experiment, this gives a calculated upper bound to the emission rate of $35 \cdot 10^3$ counts/mW/s/mm. One important approximation to note in their calculation is that they assume plane waves throughout the crystal, as the Rayleigh range in my experiment is less than one-half the length of the crystal this calculation can provide no more than an upper bound.

1.5 Sagnac Source

Having generated a pair of photons, it is necessary to entangle them in polarization. The scheme presented here was pioneered by Kim, Fiorentino, and Wong [1] in 2006.

Figure 1.2 shows a schematic of one of my implementations of this scheme: a Ti:Sapphire laser pumps a bismuth borate (BiBO: $Bi_2B_8O_{15}$) crystal that doubles the frequency. Two dichroic mirrors, each reflecting the beam five times, then dump the remaining IR light, attenuating it to no more than 0.02^{10}. A half-waveplate (HWP) is used to set the linear polarization of the pump beam so as to balance the outputs of the system: the HWP should be near $\pi/8$ from the vertical to set the polarization of the pump to be diagonal. The quarter-waveplate (QWP) is set with its fast axis vertical, and rotated about the same, to induce a phase between the horizontal and vertical components of the pump.

After passing through an IR-reflecting dichroic mirror (DM), the pump beam is incident upon a polarizing beamsplitter (PBS), where the vertical component is reflected and the horizontal transmitted. The reflected beam then passes through another HWP, which is set at $\pi/4$ from the vertical to rotate the beam from vertical to horizontal polarization. Both beams then strike the periodically poled potassium titanyl phosphate (PPKTP: $KTiOPO_4$), creating the nominal state (neglecting normalisation)

$$|\psi\rangle = (a_{h,i}^\dagger a_{v,s}^\dagger + e^{i\phi} b_{h,i}^\dagger b_{v,s}^\dagger) |\quad\rangle \tag{1.33}$$

---

[10] *i.e.* within some small interval $t \pm \delta t$. The interval is set by instrumental resolution and the bandwidths involved.

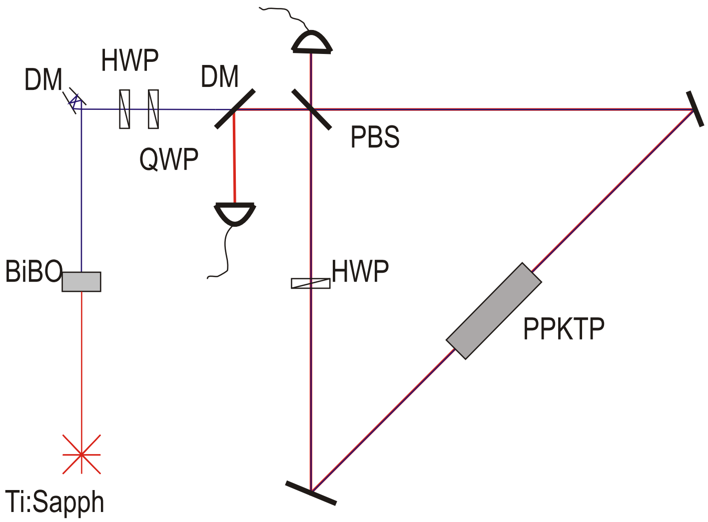

Figure 1.2: A Sagnac interferometer photon source pumped by a Ti:Sapphire laser. PPKTP and BiBO are nonlinear optical crystals, DM are dichroic mirrors, and HWP and QWP are half- and quarter-waveplates, respectively.

where the a and b creation operators are for the clockwise and counterclockwise propagating modes respectively, with the first subscript indicating the polarization and the second the frequency: s for signal photons and i for idler photons. ϕ is a phase angle, set by the various polarization optics.

The clockwise photons then strike the HWP, and undergo rotation from H to V and vice versa, yielding[11]

$$|\psi\rangle = (a^\dagger_{h,s}a^\dagger_{v,i} + e^{i\phi}b^\dagger_{h,i}b^\dagger_{v,s})\,|\quad\rangle\,. \tag{1.34}$$

All of the photons then pass through the polarising beamsplitter, reflecting the vertical photons and transmitting the horizontal ones, thus

$$|\psi\rangle = (c^\dagger_{h,s}d^\dagger_{v,i} + e^{i\phi}d^\dagger_{h,i}c^\dagger_{v,s})\,|\quad\rangle \tag{1.35}$$

where the c and d creation operators are for the vertically- and left-propagating modes (per schematic) respectively. The left-propagating mode reflects off of the DM in order to separate it from the pump.

Resolving the creation operators, my quantum state is

$$\left|\psi^\phi\right\rangle = |01\rangle + e^{i\phi}\,|10\rangle \tag{1.36}$$

where we have made the mapping $H \mapsto 0$, $V \mapsto 1$, as mentioned earlier.

For practical purposes several additional optics are inserted between the output of the Sagnac loop and the fibre couplers: a long-pass filter to remove the pump light and a polarization analyser consisting, in my case, of a quarter-waveplate and a linear polarizer.

The total system, then, is an interferometer in which a strong classical beam of light is used to produce path entangled photons, which are then interfered upon a PBS to create a polarization-entangled state with no spectral or temporal distinguishability.

---

[11] Note that the phase angle may not be consistent between equations.

Chapter 2

Prior Art

2.1 Polarization-Entangled Photon Sources

2.1.1 Postselection Sources

The simplest way to derive polarization entangled photons from SPDC is by postselection. Consider a crystal cut for degenerate collinear Type-II SPDC, where the outputs fall upon a non-polarizing 50:50 beam splitter. As the photons are distinguishable when incident upon the beam splitter, they are independently acted upon by it. Labelling the reflected mode R and the transmitted mode T, we then have the state

$$|H_T V_T\rangle + i\,|H_T V_R\rangle + i\,|H_R V_T\rangle - |H_R V_R\rangle \tag{2.1}$$

which, if we select on there being at least one photon in each of the modes R and T, yields the entangled state

$$|H_T V_R\rangle + |H_R V_T\rangle \propto \left|\Psi^+\right\rangle \tag{2.2}$$

as desired. However, there are some drawbacks to this system:

1. 50% production loss in postselection;
2. Visibility is limited by spectral distinguishability of the signal and idler beams;
3. Spatial mode discrimination requires the use of relatively small apertures;
4. In the pulsed case, four-fold events become a problem faster as power increases, as compared to non-postselected sources.

Many experiments have been done using these sources, starting with an experiment by Kiess *et al.* in 1993 [17], but they have mostly fallen by the wayside at the present time due to the above mentioned problems. As well, they also tend to have low rates, with Kuklewicz *et al.* [18] reporting 300 pairs/s/mW of pump power/nm of output bandwidth and an entanglement visibility of 99% ± 1% after subtracting accidental coincidences from their detection rates. Note that subtracting accidental coincidences from the background artificially increases visibility, and does not provide an accurate depiction of the quality of the source for uses such as quantum key distribution.

2.1.2 Cone Sources

The first true source of entangled photons (without post selection) was demonstrated by Kwiat *et al.* [19] in 1995, using quite a simple scheme: in the non-collinear case of Type-II SPDC, the two photons produced have lateral momenta relative to the pump beam that sum to zero. However, while in a birefringent crystal the extraordinarily and ordinarily polarized photons of a given wavelength are not emitted in the same direction, the degenerate emission cones for ordinary and extraordinary polarizations do overlap at two points. Whenever a photon pair is emitted along this intersection, the ordinarily and extraordinarily polarized photons can be made spectrally and temporally indistinguishable with some careful modification of the two photon modes. As they are of opposite polarizations, this yields a state of the form

$$|HV\rangle + e^{i\phi}\,|VH\rangle \tag{2.3}$$

for some phase angle ϕ tunable by the user.

Sources based on this idea, so-called 'cone' sources, have become the workhorse of single-photon quantum optics, and are used in proofs of Bell's Theorem [20], quantum key distribution [21][22], quantum computing, and so on.

2.1.3 Mach-Zehnder Interferometric Sources

This section will be brief, as these sources are similar in idea, but strictly inferior, to Sagnac interferometer based sources.

In 2004, Fiorentino *et al.* [23] reported a bidirectionally-pumped folded Mach-Zender interferometer, as shown in figure 2.1. This system eliminated spectral distinguishability from the system, as well as reducing spatial distinguishability, however it requires active servo control of the interferometer to remain stable. Even then a visibility of only 90% (after accidentals were subtracted) with 12 000 counts/sec/mW was reported. The key idea in this source, though, was that an interferometer could be used to hide path information, allowing the capture of all of the SPDC light without the need for postselection.

2.1.4 Sagnac-Type Sources

In 2006, Kim, Fiorentino, and Wong [1] demonstrated a new system for generating entangled photons using a common-path Sagnac interferometer. As shown in figure 2.2, a PPKTP crystal was pumped bidirectionally in the centre of a polarization Sagnac interferometer. One of the pump inputs is rotated by $\pi/2$ so that the pump beams have parallel polarizations. The crystal is designed so that it is quasi-phase-matched for Type-II SPDC so as to emit approximately degenerate photons collinear with the pump beam. These photons are then split upon the PBS, with one of them having passed through a waveplate rotating their polarizations by $\pi/2$. Thus the signal photons are always emitted into one output and the idler photons into the other, eliminating distinguishability on the basis of frequency.

The output biphoton state is

$$|\psi\rangle = |H_1V_2\rangle + e^{i\phi}\,|V_1H_2\rangle\,, \tag{2.4}$$

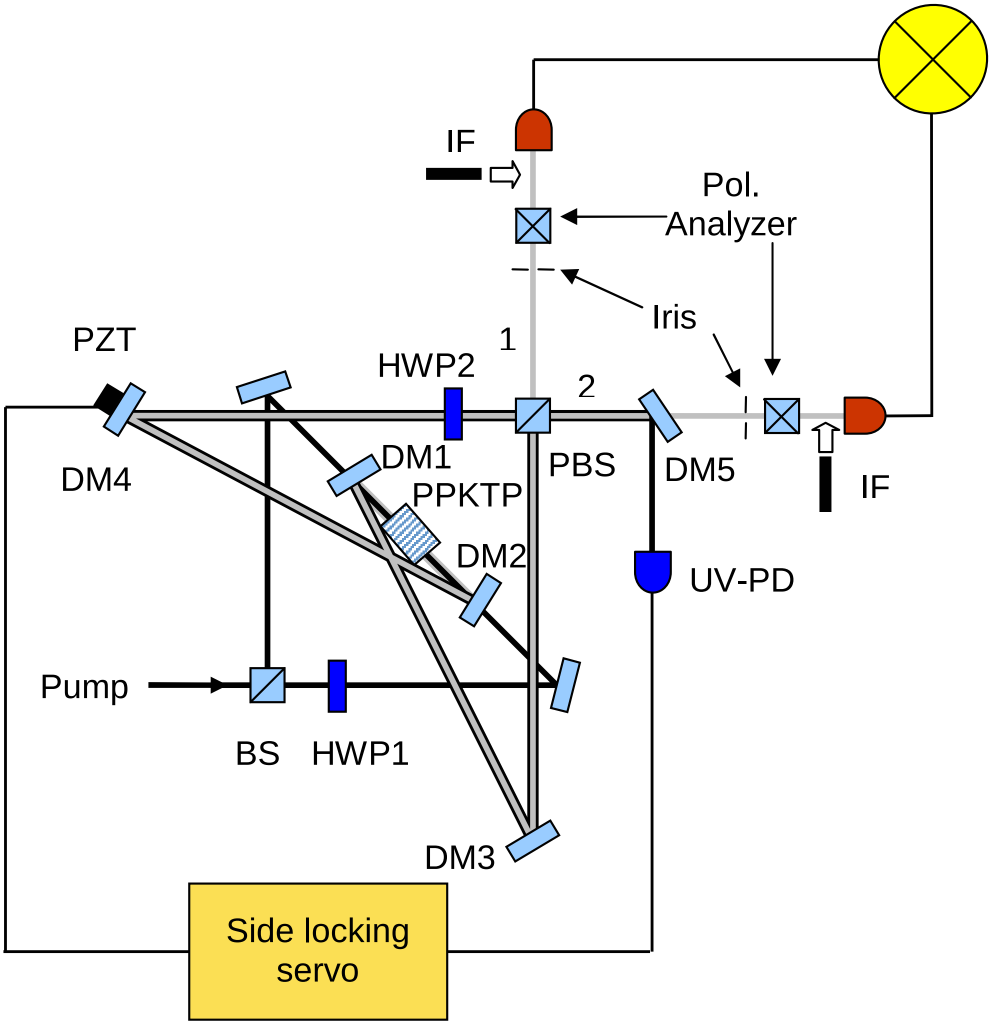

Figure 2.1: A photon pair source using a folded Mach-Zehnder interferometer. UV-PD is a power meter to monitor the interference fringes of the interferometer, which is stabilized using the side-locking servo controlling PZT. IF are interference filters, to filter out remaining pump light. This source was somewhat unstable, having a maximum interference visibility for entangled photons of 90%. Figure from [23]

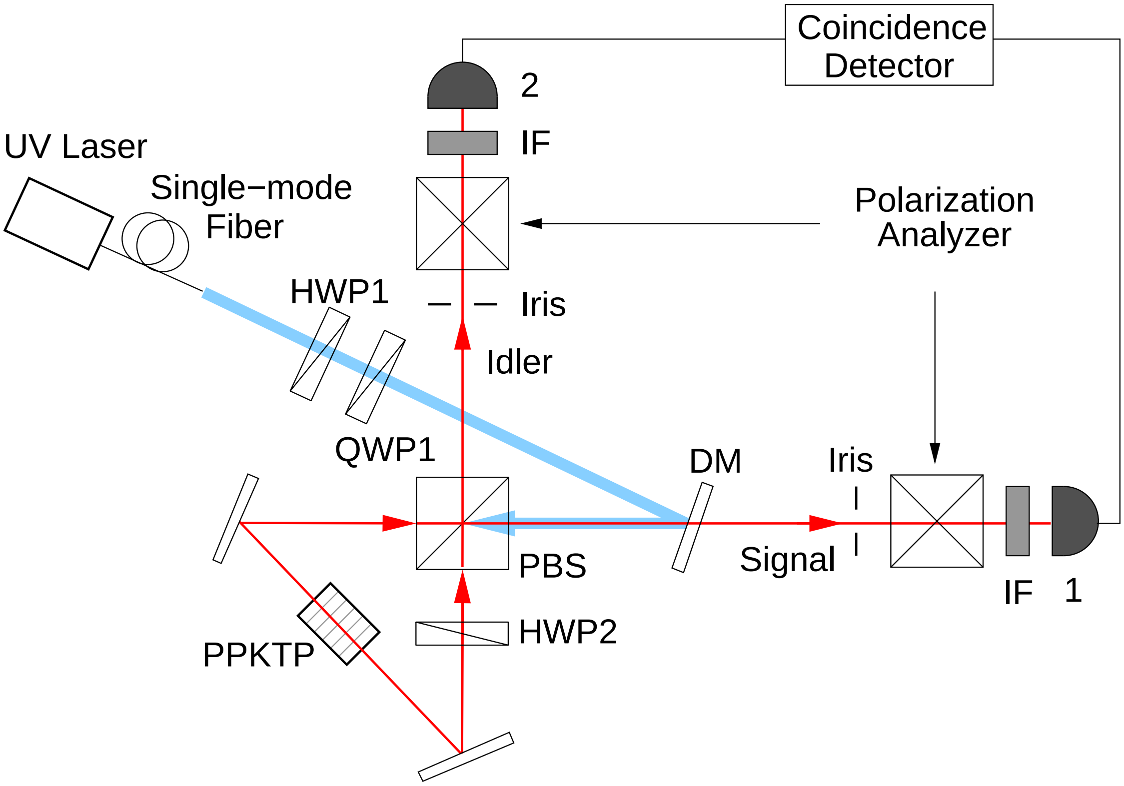

Figure 2.2: A photon pair source based on a polarization Sagnac interferometer. Photon pairs are produced in PPKTP, interfered on the PBS, and output into two detectors located at 1 and 2. Note that detection is made in free space. Figure from [1]

where the subscripts 1 and 2 refer to the two output modes, H and V are horizontally and vertically polarized photons, and ϕ is the relative phase between the two possible output states, which is determined by the phase shift induced by the waveplate in the interferometer, the polarizing beamsplitter, and the phase between horizontally and vertically polarized pump light incident on the interferometer. It is important to note that these influences do not vary with time, hence this source is phase-stable. Moreover, the phase can be tuned by inserting a waveplate into the pump beam before the beam is input into the interferometer, allowing for the selection of an arbitrary phase, typically $\pm\pi$, yielding singlet or triplet states, respectively, notated as $|\psi^{\pm}\rangle$.

This system is a simplification of their earlier work using a Mach-Zehnder interferometer, maintaining the advantages of an interferometric setup while greatly increasing stability.

The initial paper demonstrated 5000 pairs/s/mW using 1 nm of bandwidth and 3 mW of pump power, with a visibility of 96.8%, albeit with free-space detectors. Later work by Fedrizzi *et al.* [5] in Vienna improved these figures to 273 000 pairs/s/mW/nm with a tangle of $T = 0.987$ and an entanglement visibility of 99.5%.

Chapter 3

Apparatus

My experiments used several specialized pieces of apparatus; the purpose of this chapter of my thesis is to provide a sufficient description of each of these pieces that the remainder of this thesis can be understood.

3.1 Lasers

My experiments used two light sources: a continuous-wave gallium (III) nitride (GaN) laser diode at 404.2 nm from Toptica Photonics, and a picosecond-pulsed Titanium-doped Sapphire (Ti:Sapph) laser from Coherent Inc. that was frequency doubled from its fundamental wavelength at approximately 810 nm to a working wavelength of 405 nm.

3.1.1 Coherent Mira 900D

My primary light source for this experiment was a Mira 900D Ti:Sapphire laser from Coherent[1]. This is a pulsed laser system, with pulse length options of 130 fs, 2 ps, and 7 ps at a repetition rate of 76 MHz, tunable from 700-900 nm of wavelength at up to 3 W of power given the system in the lab. In the pulsed configuration used for my experiments, with 2 ps pulses, the laser ran at up to 1.5W of power, though was usually tuned to approximately 500mW for use in my experiments.

As with all Ti:Sapphire lasers, the Mira system is optically pumped, in this case with a Verdi-18W laser, also from Coherent. This is an in-cavity frequency-doubled Nd:YAG laser at up to 18 W of optical power, 60% of which was directed as pump light into the Mira with the remainder used to pump another laser in the lab.

Both the Mira and the Verdi were water cooled to dissipate the significant amount of heat generated, and to stabilize them. Unfortunately due to reasons not clear to me, the temperature stability of the cooling system was quite poor, oscillating by up to a degree and at times heating to three degrees above the set point. The likely culprit for this behavior was air in the water cooling system, but this was not fixed while the experiments were underway.

---

[1] Coherent, Inc. www.coherent.com,, Santa Clara, CA

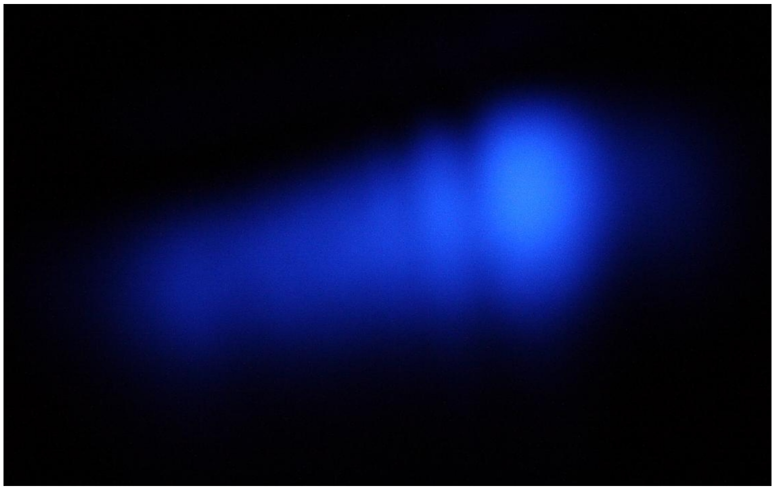

Figure 3.1: A photograph of the output of the BiBO frequency doubler. Note the sinc-like pattern in the horizontal direction. The beam was later optimized so that the brightest point was in the centre, and only this portion was used for my experiment with the rest removed using an aperture. Photograph courtesy Bill Rosgen

3.1.2 Toptica iWave

The continuous-wave laser in use for my experiment was a grating-stabilized iWave GaN laser diode from Toptica Photonics[2] at a nominal 405 nm. Unfortunately, the laser as-delivered had a wavelength of 404.2 nm, complicating my experiment as this took the degenerate phase matching temperature below room temperature (see 5.1.4). This laser operated at up to 50 mW of power, much more than neccessary for my system. However, the output power is user tunable down to 1 μW, allowing it to be set to a convienient power level: for the experiments reported in this thesis it was operated at 30 mW.

3.2 Nonlinear Optical Crystals

3.2.1 Frequency Doubling

The Ti:Sapph was frequency doubled using second harmonic generation in bismuth borate (BiBO) in a single-pass free-space setup. The BiBO crystal, from Newlight Photonics[3] was a 3 mm cube, cut for conversion from 810 nm to 405 nm. BiBO was selected for this purpose as its $\chi^{(2)}$ component for Type-I phase matching is higher than the standard crystals used for this purpose (lithium or β-barium borates), albeit with issues arising due to biaxial birefringence.

With optimal tuning, conversion efficiencies of up to 60% were attained, but for most of the experiments discussed in this thesis tuning the crystal for optimal conversion was unnecessary.

I would recommend much care be taken with the selection of BiBO as a frequency doubling crystal. As shown in figure 3.1, the laser beam emitted by my BiBO crystal

---

[2] Toptica Photonics AG, www.toptica.com, located in Munich, Germany.

[3] Newlight Photonics, www.newlightphotonics.com, located in Toronto, Canada

is significantly non-Gaussian, likely due to higher-order phase-matching solutions in the crystal—despite the rather weak (100 mm) focus used on the input beam. However, this hypothesis has not been tested. Other labs that I am aware of have also had difficulties with BiBO crystals, so I recommend avoiding BiBO without a good reason not to: the conversion efficiency is not significantly higher than that attainable with β-barium borate and if the conversion is not into a Gaussian or at least nearly Gaussian mode, it then is not only useless but detrimental.

3.2.2 Spontaneous Parametric Down-Conversion

In this experiment spontaneous parametric down-conversion (SPDC) was performed in a flux-grown periodically poled potassium titanyl phosphate (PPKTP : $KTiOPO_4$) crystal from Raicol Crystals[4].

KTP is a relatively high damage threshold nonlinear optical crystal with both Type I and II conversions available, traditionally used for high-power frequency doubling to the green region. In its periodically-poled form is a common component in optical parametric oscillators (OPOs), and has been used in sources of photons in quantum optics since at least 2000 [24], and is the most common choice[5] for applications requiring collinear Type-II SPDC.

However, to my knowledge none of these applications have been made with ultrashort[6]: the present experiments were designed, in part, to determine the utility of PPKTP, and the photon sources dependent upon it, with a ultrashort pulsed laser. Concerns included laser-induced damage and temporal (longitudinal) walk-off: the latter will be discussed in detail in the experimental design section. While KTP has a very high damage threshold for a nonlinear optical crystal, 80 MW/cm^2 with a Q-switched 532 nm laser switched at 10 Hz with 10 ns pulses[25], the periodically poled version of this crystal has a much lower damage threshold due to the interfaces of the two differently oriented regions providing the grating. Moreover, the usual operating wavelengths for KTP are significantly longer than the wavelengths used in this experiment (633 nm instead of 405 nm). The violet is a highly dispersive regime for PPKTP, leading to a higher propensity for grey tracking (see section 4.2.3). Unfortunately, there is no good data published on the damage threshold for KTP at the wavelength used in this experiment, and the Sellmeier equations for prediction of optical properties are known to perform poorly in this region. This will adversely affect some of the theoretical predictions in this thesis.

3.3 Linear Optics

Thorlabs[7] provided most of the standard optical components in my experiments, including the mirrors, all of which were silver to reduce polarization dependence, and the lenses, which were fused silica insofar as possible to reduce fluorescence due to the violet pump beam.

---

[4] Raicol Crystals, Inc., www.raicol.com, Israel.

[5] In fact, PPKTP is the only crystal I know to be used for this purpose.

[6] Ultrashort here meaning pulse lengths on the order of picoseconds or less

[7] Thorlabs, www.thorlabs.com, Newton, NJ, USA

The polarizing beamsplitter used in the Sagnac interferometer was provided by CVI[8] with a design wavelength of 810nm and thus peak performance thereat. As some of my experiments took place at other wavelengths, the degradation of performance as the wavelength shifts is important. The PBS used performed relatively poorly at the pump wavelength of 405 nm, especially in reflection, with about 30% incorrect reflection. However, this is not a large concern: while it adversely affects the efficiency of the source it does not reduce the quality of the photon pairs produced, and having sufficient laser power was not a concern in this experiment. The primary adverse affect of the poor performance of the beamsplitter is that it exposes the somewhat fragile PPKTP crystal to unnecessary laser flux, which increases the potential damage.

All the filters used in the final experiment were long-pass filters made of coloured Schott glass, obtained from Präzisions Glas & Optik[9] in 3 mm thick portions, two of which were used per arm of the experiment. Unfortunately, these were not AR-coated, leading to significant unanticipated losses due to the filters.

The fibre optics used in the experiment were 3 m single mode SM810 fibres with FC-PC connectors from O-m6[10]. This supplier was chosen as they could supply use with black-patch fibre optics, which greatly reduce absorption of light from the environment into the fibre optic, reducing our experimental background. Performance of the system was not greatly reduced if the room lights were on, due primarily to these fibres.

3.3.1 Custom Optics

However, our dichroic mirrors were custom made as the specifications required for the dual-Sagnac approach were quite high: less than 1% incorrect transmission and reflection. Therefore, custom mirrors were ordered from local supplier VacuLayer[11], with both the dual dichroic mirrors for the apparatus, coated to reflect 810 nm light from the front surface and 405 nm light from the back surface at an angle of incidence of $\pi/8$, and mirrors coated only on one side for general use.

Unfortunately, they were unable to meet specifications for the blue-reflecting dichroic mirrors, so that coating was made by Precision Photonics[12], who were very quick in doing so. Figure 3.2 shows the performance of the blue DM coating at $\pi/8$ incidence.

3.4 Optomechanics

The majority of the mounts in my experiment are stock parts from Thorlabs. All of the translation stages are New Focus[13] Gothic Arch translation stages in various sizes, and the rotation stages for the interferometer's beamsplitters are Standa's[14] 50M101T "miniature tilt/rotation mount of side control", which is a small footprint two-axis stage with both degrees of freedom accessible from the top of the mount. Unfortunately, the

---

[8] CVI Melles Griot,, www.cvilaser.com, Albuquerque, NM, USA

[9] Präzisions Glas und Optik GmbH,, www.pgo-online.com, Langen, Germany. Since this purchase domestic suppliers have started carrying the part used in my experiment.

[10] O-m6 Technologies, Inc., www.om6.com, Mirabel, PQ

[11] VacuLayer, Corp., www.vaculayer.com, Georgetown, ON.

[12] Precision Photonics, Corporation, www.precisionphotonics.com, Boulder, CO, USA.

[13] New Focus, www.newfocus.com, San Jose, CA, USA.

[14] Standa Ltd., www.standa.lt, Vilnius, Lithuania.

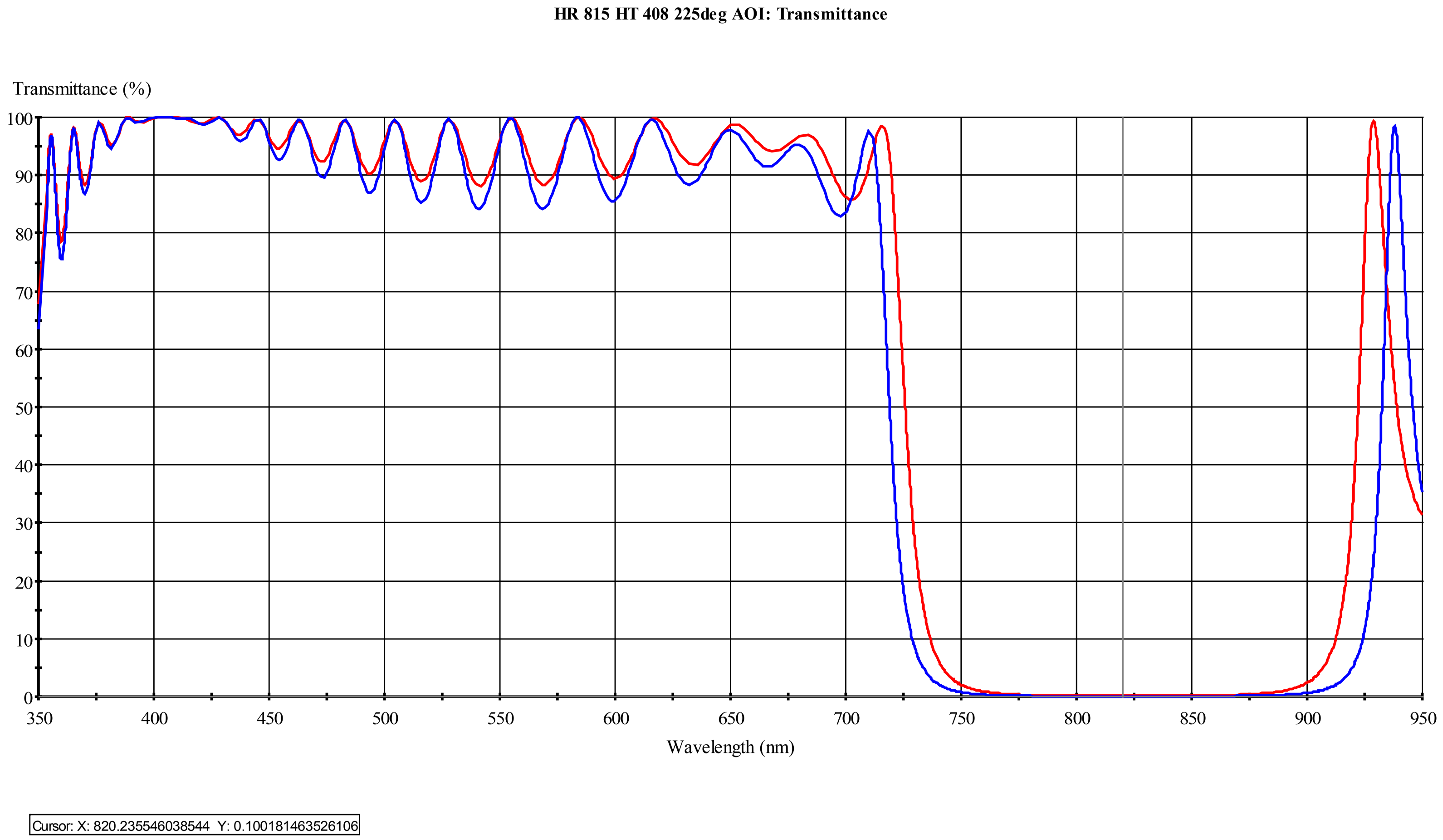

Figure 3.2: The transmission model provided by Precision Photonics for the custom 405 nm reflecting dichroic mirrors. Red is p-polarized and blue is s-polarized light.

rotation degree of freedom is hysteretic cross-coupled, shifting the mounted object in the tilt degree of freedom upon reversal of the screwing direction.

3.4.1 Fibre Couplers

The fibre coupling system employed consists of two 60 mm square New Focus stages to which New Focus' model 9091 fiber positioner was mounted with homemade brackets. A 10X microscope objective was used to focus light into the single mode fibre optic.

I strongly recommend this system or something similar for fibre coupling. During the course of experimental design and optimization several other systems were tried, generally revolving around a Thorlabs SM1ZH zoom housing, a mirror mount, and a microscope objective. While significantly cheaper to implement, at about half the cost, the crosstalk between degrees of freedom and hysteresis in the zoom were sufficient to make alignment of the system extremely difficult, and the stability nonideal. It would be preferable to find a system that exhibited the nice features of the New Focus 9091 system without being quite as large, especially as the 9091 coupler is in many senses overkill: the fine-tune on the system is so fine that it is rarely useful, for instance. It also has 'extra' degrees of freedom that are rarely used, such as the tilt of the fibre tip. Unfortunately, I am not aware at this time of any such system.

3.5 Electronics

On the whole, the electronics for these experiments were, fairly simple. Power readings were taken with an assortment of power meters, which will be specified as I report the results. Otherwise, there were only two electronic components: silicon single photon avalanche diodes (SPADs), which were stock Perkin & Elmer quad units, and a timetagger, which takes TTL input and outputs an event time and channel via USB with a resolution of $(6.4\text{ GHz})^{-1}$. Unfortunately for high-power experimentation, this timetagger saturates at about 2 million counts/second (instantaneous) and the average output cannot exceed USB speeds, or in practice about 1.2 million counts/second. Above this rate, counts are dropped, and worse yet, coincident counts are more likely to get dropped due to a FIFO buffer, leading both low to singles on the electronically later channel and an apparently bad coincidence rate. Fortunately, this behaviour can be easy to spot by simply blocking one channel (optically): if the count rates in the other channel are appreciably altered, then counts are being dropped by the timetag system.

The time precision of this system is $(6.4\text{ GHz})^{-1}$, however the clock speed is only 640 MHz, with the output having 10× upsampled resolution. It does not, however, have quite that much accuracy as the relative timing of the apparently coincident events can differ by up to a nanosecond. This can only be attributable to variances in the electronic equipment as the optical path lengths in the system do not vary by more than tens of picoseconds. As we can simply take all events whose timing delay is less than some interval and declare them coincident, the only effect the electronic jitter causes is to restrict how tightly we can constrain events to be coincident and thus what level of background is endured.

The SPADs, timetagger, and support electronics are contained in a simple package assembled by Zhenwen Wang, an electronics support technician for Science Technical Services at the university.

3.6 Computers and Computing

Generally, the final step in any modern experiment is computerizing and processing all of the data. In my case, the computer in question was a Dell Vostro 1500 laptop, which was used to control the laser diode and receive data from the aforementioned timetagger unit.

The collected data was then processed using one of several homemade programmes:

- A C#-based system derived from the code used by Chris Erven in his quantum key distribution system [26]. This code was modified to allow for variable timing windows, but due to difficulties in extending it further was superseded in use by the programme below. While very functional for the purposes for which it was written, it was not ideal for mine.
- A Labview/C++ based system written primarily by Prof. Gregor Weihs. I added tracking plots for the coincidence rate and the conditional coupling rate for each channel to simplify alignment, and also added code to save the data from each time interval to a file for later use in analysis. I also removed some functionality that was unnecessary for my experiment: for instance, three-channel coincidence track that was not needed for my two photon experiment. This system worked quite well, though as with any code further improvements could be made: if closed improperly it crashes on restart; and it is unresponsive if the counting interval is set to tens of seconds. However, neither of these flaws is fatal, and given the amount of time necessary to fix them I decided not to.

The latter programme declares two events coincident if they occur within a user-tunable number of nanoseconds (for my experiment set to 1 ns, with the zero offset tunable by the user. Surprisingly, given the nearly equal optical and electronic path lengths in my experiment this offset was significant: 4.35 ns on one of our sets of detectors and 8.4 ns on another. This can only be attributable to electronic delays in the detector/timetagger complex, though the provenance of them is unclear. Fortunately, for any given set of detectors this offset appears to be constant, and can simply be set-and-forgot.

Chapter 4

Experimental Design

So far I have shown the various components and ideas leading to my project, but the experiments have not been explained in detail. In this chapter, I will provide a thorough explanation thereof and detail the various revisions and improvements made to the initial proposal to become the final experiments.

4.1 Initial Proposal

The initial goal of this project was twofold: to test the feasibility of Sagnac-type sources in a pulsed configuration so as to enable multi-fold experiments, and to explore a slightly different configuration of the interferometer.

4.1.1 Dual Sagnac

The standard design, shown again in figure 4.1, consists of one interferometer loop with one nominally-polarizing beamsplitter used for both the pump and the down-converted light.

The polarizing performance is optimized for the single-photon wavelength(s), while any stock polarizing beamsplitter (PBS) will have significantly degraded performance at the pump wavelength. The approach taken by Fedrizzi *et al.* was to obtain custom beamsplitters designed for dual-wavelength performance. I sought to avoid this expense by substituting dichroic mirrors in the following manner:

1. Replace the mirrors in the interferometer with dichroic mirrors coated to reflect the pump beam off of the back surface and the down-converted beams off the front surface. Given that these mirrors are not at normal incidence, this separates copropagating beams into two parallel beams.
2. Add a second beamsplitter designed specifically for the pump beam's wavelength. In the original design for my experiment this was a 50:50 non-polarizing beamsplitter, but, due to alignment imperfections, using a polarizing beamsplitter in this position is a better idea, allowing for the two pumping directions to be balanced. Note that this brings a number of additional degrees of freedom into the experiment—the relative angle and lateral position of the two beamsplitters must be controlled precisely, while the remaining additional degrees of freedom are less important.

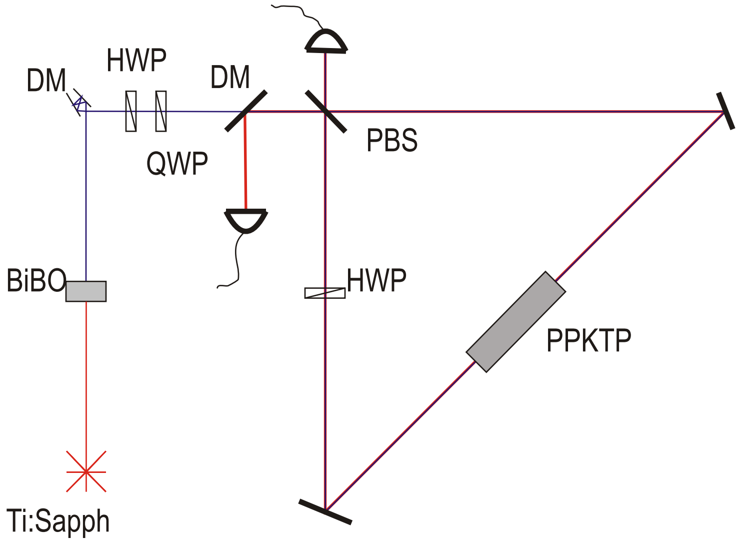

Figure 4.1: A schematic of a Sagnac interferometer-based photon pair source. Red lines are 810 nm, blue are 405 nm. DM are dichroic mirrors, HWP and QWP are half- and quarter-waveplates.

3. Use single-wavelength waveplates for each of the pump and the down-converted light. As the two colours of light are now separated at this location in the interferometer, this is feasible, however the beams are not very far apart (2.5 mm), so using traditional mounts is impossible. The simplest solution is to buy waveplates with holes drilled in them, which was the solution I adopted. Alternatives include using mounts that do not completely surround the waveplate.

4. Separate the pump and down-converted beams after they exit the interferometer using a simple mirror. After doing so, any residual pump light can be removed using a filter. Note that less filtering is necessary than in the standard design, as more than 99% of the pump has already been removed by the dichroic mirrors. Unfortunately, as the ratio of pump to down-converted light in an SPDC process is on the order of a billion to one, extensive filtering is still required.

The end result is shown in Figure 4.2: two triangular Sagnac interferometers sharing one common side including the PPKTP crystal and having two sides parallel but not collinear, with the outer one for the pump wavelength and the inner for the down-converted wavelength. It was hoped that the resilience of Sagnac interferometers to disturbances would be carried over to this dual Sagnac design as the path lengths between the two interferometers would have to change on the order of the transit time of a photon through the loop in order to affect the entangled state produced.

4.1.2 Pulsed Sagnac

The second major goal of my experiment was to demonstrate the feasibility of Sagnac-type sources for multi-photon experiments by demonstrating their viability when used with a pulsed laser. In future, the final source will be duplicated in order to demonstrate

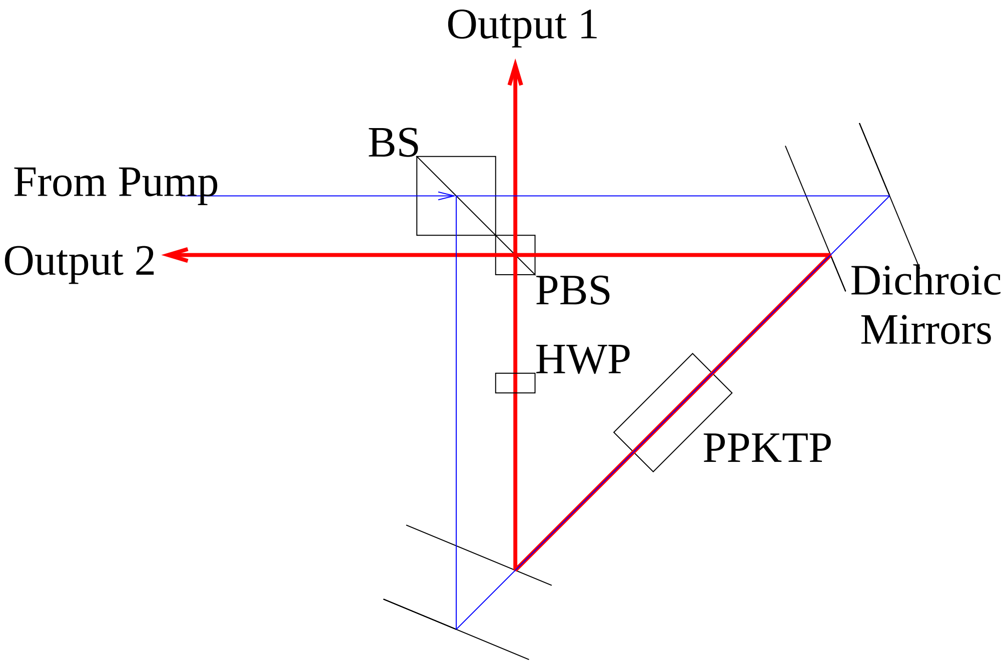

Figure 4.2: A schematic for a dual Sagnac interferometer-based photon pair source. The separation of the two colours in some of the interferometer allows them to be controlled independently. Unfortunately, sufficiently coupling remains between different degrees of freedom to make this source very hard to align.

entanglement swapping between them. Disappointingly, time limitations have caused that experiment to be removed from the scope of this thesis: it remains in the planning stages.

As of the commencement of this project, the only demonstrated Sagnac type sources were pumped with a low-power GaN laser diode, and it was not clear such a source would work well with an ultrafast laser. After the start of the current project, Kuzucu and Wong [4] demonstrated in 2007 a pulsed Sagnac source with a Q-switched frequency-quadrupled fibre laser. However, the pulse length in that experiment was 50 ns, which made it both quasi-continuous-wave and unsuitable for multi-photon experiments.

Three serious obstacles lie in the way of simply substituting a Sagnac interferometer source into a standard femtosecond-laser-pumped multi-photon experiment:

1. High Dispersion: Due to the high dispersion of PPKTP in the violet region, the degeneracy splitting $\Delta\omega = \omega_s - \omega_i$ changes quite rapidly with the pump wavelength, at a rate of about 20 nm of splitting per nanometre of pump wavelength change. Therefore, as in a typical femtosecond laser the output bandwidth of the SPDC crystal is quite wide with respect to the bandwidth of the laser; thus the standard method of filtering the output down to the bandwidth of the pump in order to eliminate timing information will remove a large fraction of the desired signal photons.

2. Laser-induced damage: Grey-tracking, the damage mechanism in PPKTP [27], is a process wherein lattice ions are optically displaced and form dislocations; creating the visible optical tracks for which the process is named. It turns out that below

some saturation power, which is quite high (and not known for 405 nm light), that this damage scales with peak power: hence short excitation times lead to greater tracking. Once damage has been induced, these grey tracks fluoresce, decreasing the signal-to-noise ratio, making the system harder to align, and putting a maximum on the amount of signal that can be seen without damaging the detectors or in our case saturating our timing card. [1]

3. Timing jitter: Most fatally, the timing jitter induced by the centimetres long crystals is several picoseconds. At 405 nm/810 nm, the group velocities of the signal, idler, and pump are $c/1.907, c/1.806$, and $c/2.106$ [28] respectively, leading to an absolute timing jitter relative to the pump of 1.00 ps/mm. Even if the entire length of the crystal does not participate in SPDC equally, there is very little point in using a 10 mm or longer crystal with a femtosecond excitation to pump a multi-photon experiment[2].

Having examined femtosecond pulses and deciding against them, I examined picosecond pulsed ultrafast lasers as a possible pump for my photon source. With respect to the three concerns above: the first is lessened, though narrow filters will still be necessary; the second is reduced, but is still a concern, and I will discuss repair and mitigation strategies in section 4.2.3; and the third provides an impetus for using such a pulse length. As a result, for my experimental demonstration a pulse length of 2 ps was chosen from amongst those readily available in our lab: 130 fs, 2 ps, and 7 ps.

4.2 Implementation

4.2.1 Focusing/Coupling

One minor, but time-consuming, detail in the design of a Sagnac-type source is the design of the focusing elements on both the input and output sides of the source. For simplicity all such designs operating in free space have kept all lenses outside the interferometer loop. Due to a lack of suitable polarizing in-fibre beamsplitters, variants of these sources based on the exploitation of the $\chi^{(3)}$ nonlinearity of optical fibre have had to fibre-couple inside the interferometer.

However, for work in free space, shifting the lenses outside the loop saves significant headaches: the nonlinear beam steering of focusing elements need not be dealt with as the interferometer is tuned. As a rule of thumb, there are two goals in the choice of focal properties:

1. For optimal coupling, the waist of the down-converted beam should be $\sqrt{2}$ times the waist of the pump beam. [5][16]

2. The waist of the pump beam must be optimized based on the length of the crystal. Theoretical results by Ljunggren [29], showed an optimum at $\approx 2.0 \pm 0.4$ Rayleigh

---

[1] In private communications, both Alessandro Fedrizzi and Thomas Jennewein have indicated that an attempt at driving PPKTP with femtosecond excitations failed due to this problem.

[2] Note that using a very short crystal is possible in this type of source(and may in fact work quite well) but this throws away one of the benefits of Sagnac-type photon sources: namely the longer interaction length in the crystal.

ranges contained in the crystal. Experimental results [5] have reinforced these conclusions, albeit finding a weak dependence on the length of the crystal: as the crystal lengthens the optimal focus tends to be tighten, nearer 2.4 than 2 Rayleigh ranges in the crystal, with the optimal beam waist approaching an approximately constant 25 μm

The combination of the preceding two criteria constrains the beam shape both into and out of the crystal. The goal, then, is to achieve that beam shape with a maximum of ease.

Ideally, two lenses anywhere before the interferometer in setup before the interferometer can achieve the desired beam profile. It is unlikely that just one will work, as the required e^{-2} beam diameter at the entrance to the interferometer is several millimetres, depending on the size of interferometer and the length of the crystal. In my case, the beam diameter was about 3 mm. A 200 mm focal-length lens placed at $\sim$225 mm from the center of the interferometer, combined with a slightly divergent beam incident on said lens, achieved the design beam waist of 22 μm.

For the output beams, an obvious simplification is to ensure that the same optics can be used in both arms by symmetrizing them insofar as possible: this primarily consists of placing the coupler for the signal beam at an equal distance to the interferometer as the couple for the idler beam.

Having done so, one can typically find a microscope objective and a distance to the interferometer that conjugates the in-crystal focus into the mode of a single-mode fibre. In my case, this turned out to be a 10X objective and a distance of 280 ± 10 mm, with the fibre at approximately the rated working distance from the micrometer.

Note that throughout this subsection the optimization was performed for a 10 mm crystal, and that this crystal was later replaced with a 15 mm one, as the first crystal was broken. This is unfortunate as the focal parameters could be reoptimized for the longer crystal, but should not reduce absolute performance from the 10 mm crystal.

4.2.2 Alignment

Aligning a Sagnac source is a relatively new problem, as they were first developed only three years ago. I will first describe the procedure I developed to align a standard one-beamsplitter Sagnac source, and then explain the differences and difficulties of going to a dual Sagnac system.

A Sagnac interferometer is an unusual device to align in optics because all of the optics have at least two beams incident upon them. Isolating the two directions from each other is not possible, so a different approach must be taken.

My alignment procedure for the interferometer was as follows:

1. Align the input beam to some pinholes, preferably fixed along a row of holes of the table and dead level.

2. Place a half-waveplate (HWP) in the beam to ease the remaining alignment steps: this waveplate will be ultimately necessary for tuning the output state of the source. Try to ensure that the HWP is normal to the beam; this may not be completely possible, as waveplates often seem to be mounted a degree or two crooked, leading

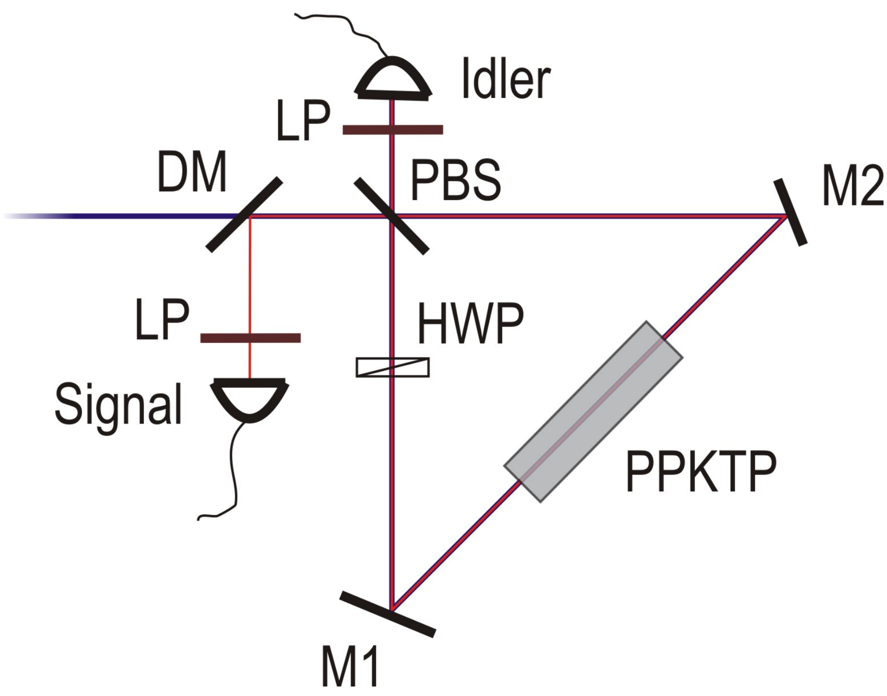

Figure 4.3: Detail schematic of my Sagnac source. Optics are labeled for reference.

to the beam wobbling as it is passed through the waveplate. If this is the case, try not to rotate the HWP more than necessary from the global optimum.

3. Place the focusing optic for the interferometer in the pump beam. Ensure that it is centred. I strongly recommend that it be placed on a longitudinal translation stage so as to allow later adjustment of the location of the focus.

4. Insert the dichroic mirror that will later separate the pump beam from the idler beam. This must be done now as this mirror displaces the pump beam by several millimetres. This mirror need not be easily adjustable, but ensure that it is level and solid, and that there is space for the necessary optics and the fibre coupler in the notional beamline.

5. Insert the polarizing beamsplitter into the pump beam. Insofar as possible, the reflection should be at $\pi/2$ to the pump beam, but a slight misalignment here is not critical.

6. Place the interferometer mirrors with angles of incidence of $\pi/8$. These should be placed such that the beam between them is above a row of holes on the table. Some pinholes placed for prealignment of these mirrors are recommended, but note that beginning with the next step they cannot be treated as the canonical location of the beam as there are insufficient degrees of freedom for both directions to be aligned to these pinholes in a simple manner.

7. Prealign the interferometer by aligning the pump beam *at* the mirrors. Silver mirrors are lossy enough that, given a sufficiently strong pump beam, one can see the locations at which they reflec: if the two counter-propagating beams are perfectly overlapped at both mirrors then they should be exactly anticollinear. If

the beamsplitter has translational or rotational degrees of freedom, those can be adjusted here to centre the beam on the pinholes inside the interferometer, but this is not necessary.

8. In the output arm of the interferometer, insert a UV polarizer set to diagonal polarization[3]. Ensure the pump beam is also set to diagonal polarization. Direct the output beam to fall upon a screen, preferably at a distance of several metres. Interference fringes should be apparent, if not, go back to the previous step until they appear.
9. Using the two interferometer mirrors, tune the position of the beam such that the fringes are optimized. As the interferometer nears to perfect alignment, the fringes widen: near perfect alignment the beam should very nearly disappear and do so symmetrically. Note that if one of the waveplate or the polarizer are out by $\pi/2$ there will be a bright instead of dim spot: flipping either one will solve this problem.
10. Ensure that the two mirrors for the counter-propagating beams still reflect the laser at the same spot; occasionally one can misalign the system in such a way as to have an apparently good fringe pattern but still have a badly aligned interferometer.
11. Insert the dual-wavelength HWP into the interferometer. Tune it to flip the polarization of the pump beam as it passes through it: this is most easily done by setting the input pump beam to one of horizontal or vertical and then minimizing the output of the interferometer. All of the input light should exit the interferometer via the input port when this waveplate is tuned optimally. Note this position as this HWP will be adjusted more than once in the future.
12. Remove the UV polarizer from the output arm and place the fibre coupling system in its design location. Back-align this fibre coupler with 405 nm light to the pinhole placed in the input beam earlier. Switch to 810 nm light, if available, to tune the position of the focus to be in the centre of the interferometer. This is most easily checked near the beamsplitter, where the size of the ingoing and outgoing beams can be compared to ensure their equality.
13. Maximize the amount of pump light coupled into the fibre by beamwalking, but do *not* adjust the focus. The optimal focal distances for 405 nm and 810 nm light are sufficiently different that optimizing the focus here is detrimental to achieving optimal coupling.
14. Place the fibre coupler for the idler beam into place, and align it to the first fibre coupler. For preliminary alignment, back-aligning this coupler to the pump beam inside the interferometer can be done, but as there is a dichroic mirror in the system the pinholes in the input are inaccessible. Tune this coupler using 810 nm light to maximize transmission into the first fibre coupler, so that at worst the two fibres are looking at each other. Note that here one can adjust the focus on the idler fibre coupler: any misalignment in the zoom of the two couplers will therefore be of opposite sign hereafter.

---

[3] It is important to note here that many visible or IR wavelength polarizers behave unpredictably in UV light: the Thorlabs LPVIS models, in particular, are weakly polarizing at 405 nm in the direction opposite to the nominal polarization direction. While this does not matter for this alignment step except to weaken the visibility of the fringes, it is something that one should be aware of.

15. Place the filters into the beam; my system used 6 mm of LG715 filter glass per arm, which induces a significant amount of parallax. Try to align the filters to be normal to the beam, and then correct the position of the fibre couplers to maximize coupler-to-coupler transmission. As the signal beam is better aligned, I recommend putting the filters in that beam first, and then those for the idler. These filters should be mounted on flip mounts as they will be inserted and removed from the system repeatedly; if the light is going to reënter free space before being detected then they can be omitted at this point and relocated there.

16. Insert the PPKTP crystal into the system. Without touching the fibre couplers, optimize transmission from coupler-to-coupler through the crystal. Lateral and vertical adjustment, as well as pitch and yaw are necessary to reach the global optimum. The translations are helpful as the poling interfaces are not all optically clean and flat, so many possible beam paths badly distort the beam; looking at the beam profile directly, using a business card or a similar item, can help to find a good section of the crystal to use.

17. Realign the fibre couplers: the signal beam to the pump and the idler couplers to the signal coupler. These should be relatively minor adjustments. Note that the crystal has increased the optical length of the interferometer by twice its physical length as the index of refraction of KTP is about 3; this will affect all the foci in the system. The pump focus can be adjusted now, but I would recommend deferring adjustment of the fibre couplers until detecting SPDC photons.

18. Connect the two fibre couplers to the single photon detectors and turn on the pump beam. Coincidences should be present at this point: ensure that they are present for both of the pumping directions by turning the HWP dedicated to that purpose.

19. Insert a polarization analyzer into both arms to aid in fine tuning. Note that this can be done in step 15, above, if desired. I found that in my case the polarizers shifted the beam by about 50 μm, so I left them in place nearly permanently. Again, when reöptimizing after inserting the polarizer, do not adjust the angle; adjust only the position of the fibre coupler.

20. Locate the optima for VH and HV, that is for pumping in both the clockwise or anticlockwise directions, without tuning the angle degree of freedom of the couplers. Average these optima and set the coupler to this position.

21. Either remove the polarization analysers or set them to one of the entangled bases ($|\pm\rangle$ or $|\pm i\rangle$); if the latter check both the correlated and the anticorrelated setting: depending on the input polarization one of these should be much larger than the other, giving the phase in the nominal state $|HV\rangle \pm |VH\rangle$. The counts in the entangled basis should be nearly equal to the counts in the two standard bases.

22. Optimize the count rates in the chosen entangled basis by beamwalking. The zoom of the coupler can also be optimized here; attempt to optimize the directional degrees of freedom before optimizing the zoom to ensure that the focus is getting tighter, not looser.

23. Check the visibility of entanglement and the coupling rate; if these are sufficient for experimentation then proceed thereto, while if they are marginal then continue

with step 24. Often, to reach even marginal experimental viability several iterations of steps 20 through 22 are necessary before continuing.

However: If the distance between the HV and VH beams is large (*i.e* 50 μm or greater) the interferometer is slightly misaligned, and its alignment must be improved by the following procedure. Be aware that this is a slightly risky procedure—if care is not taken returning to alignment of the interferometer by its fringes may be necessary (see step 9).

(a) Set the signal channel to H and the idler channel to V. Tune mirror 1 (see figure 4.3) to maximize coincidences between the channels. Monitor the singles for each channel; ideally, they should both peak at the same position.

(b) Set the signal channel to V and the idler to H. Tune mirror 2 to maximize coincidences.

(c) Repeat steps 23a and 23b until the two directions are nearly identical. Then tune to an entangled basis ($|\pm\rangle$ or $|\pm i\rangle$) and check the contrast. Tune the interferometer very slightly to find a maximum in this basis. At this point, another iteration or two of steps 20 to 22 should result in a marginally working source.

24. The balance between the HV and VH count rates can be adjusted by tuning the insertion HWP. This should not need adjustment by more than 5°.

25. Adjustment of the phase between the signal and idler beams can be accomplished with a birefringent material inserted in the input beam and rotated about the vertical axis, with the fast axis mounted either vertically or horizontally. In the literature—as well as in my experiment—a zero-order QWP was used for this purpose, but this must be mounted at a significant angle (more than 10 degrees to normal incidence) to effect zero relative phase between the horizontal and vertical polarizations, inducing spatial separation between the horizontal and vertical beams. A QWP must be mounted at this large angle as the Sagnac source is nearly at the correct phase before the insertion of the phase-adjusting optic, so the $\pi/4$ phase induced by the QWP at normal incidence is unhelpful.

    By contrast, a HWP[4] would just flip $|+\rangle$ for $|-\rangle$, an acceptable outcome. A multi-order optic would also have the advantage of requiring a smaller angle of incidence to induce an equivalent phase, inducing less parallax.

26. Having adjusted the phase to maximize contrast in the basis of choice, the interferometer will be slightly misaligned and imbalanced HV to VH, and so must be realigned; typically only lateral adjustments of the fibre couplers and adjustment of the H to V balance of the pump is necessary, but this of course affects the phase angle. Several iterations of this will result in optimal visibility.

Before switching to a conventional Sagnac interferometer, I attempted to construct and use, as mentioned previously, a dual Sagnac configuration; this design proved to

---

[4] Better yet, a unit waveplate would, at normal incidence, do nothing, yet could be slightly misaligned to add a very slight phase. Note that in any case rotating a waveplate about an axis normal to the table will only add phase of one sign: if the opposite sign is needed the waveplate must be rotated by $\pi/2$.

be very difficult to work with. One of the key steps in aligning a Sagnac source is the alignment of the couplers to the pump beam, which guarantees that the fibre mode overlaps the collinear down-conversion mode. Splitting the beamsplitter in two, one for each of the pump and down-converted modes, adds an additional two degrees of freedom that must be precisely tuned: the relative angle and lateral position of the two beamsplitters. This effectively changes a problem where two beams must be precisely aligned (the two pump beams) and makes it into a problem where four beams must be precisely aligned: in some sense these are the two pump beams after being split on both beamsplitters.

This increase in alignment difficulty is made worse because the beams are all interdependent; there are no experimentalist-accessible degrees of freedom that only affect one of the beams. Note that this design is, in some sense, a folded Mach-Zehnder interferometer where the steering mirrors are common to both beam paths: this increases stability at a cost of experimental difficulty.

Many months were spent attempting to find a good way to align this dual Sagnac design to little result, while the conventional design produced preliminary results after a week's time. Furthermore, the dual Sagnac approach does not clearly demonstrate significant improvements over the standard design. The primary reason for this design was to avoid the necessity of a dual-wavelength beamsplitter and half-waveplate; yet the latter is easy to acquire and the former is not a major concern. If the PBS is optimized for the down-conversion wavelengths then the states produced will be of high quality; while poor performance at the pump wavelength will reduce the efficiency, in terms of photons of down conversion per pump photon used, it will not affect the states produced. Poor pump performance is unfortunate as the damage to the crystal scales like the total pump power, limiting the number of photons that can be produced, however, it is not criticial. A custom made beamsplitter operating at both 405 nm and 810 nm would be sufficient to ideally solve this problem. Given that the dual Sagnac design required the production of custom dichroic mirrors at moderate expense, and that the production of a custom beamsplitter is not significantly more expensive, even the cost argument for the dual Sagnac design is weak.

My recommendation, and one of the primary results of this thesis, is that this design be avoided as both difficult and unnecessary. Having come to this conclusion, I changed the design used to that of a standard Sagnac source so as to meet the other major goal of this thesis: evaluating the viability of making a pulsed Sagnac source.

4.2.3 Grey tracking

KTP is known to have a quite high damage threshold: some 80 MW/cm^2 with a Q-switched 532 nm laser switched at 10 Hz with 10 ns pulses[25]; PPKTP at 405 nm is unfortunately weaker and suffers from low-level damage at the powers in use in my experiment.

The symptoms of grey-tracking in KTP are the creation of fluorescent centres in the crystal as nuclei are dislocated from their equilibrium position in the crystal lattice. It is this mechanism that facilitates damage in PPKTP as the interface between each poling direction is a crystal grain boundary. As damage accrues, the crystal becomes gradually more opaque to the laser light and fluoresces; the fluorescence is obvious on SPADs, especially in a pulsed configuration, and on a spectrometer as a broadband background (see section 5.1.3). The amount of fluorescence increases gradually over time as low-level damage accumulates.

Fortunately, due to the damage mechanism involved the damage is largely reversible: if the crystal is heated above 180°C and held there for four hours or more the crystal structure relaxes to its ground state [27]. I have used this procedure several times to repair my crystals, and it works quite well. Note that to avoid cracking the crystals and damaging the coatings Raicol, our crystal supplier, recommended that at temperatures above 80°C the temperature change no more than 10 °C/h, a suggestion which I followed.

Studies, such as that in Boulanger and his coworkers' paper [27], have shown that the rate at which damage accumulates in a KTP crystal decreases as temperature increases, which is limited by the safe operating temperatures for the crystals and their coatings; this suggests that a good mitigating strategy to reduce or eliminate grey-tracking in a PPKTP source would be to design a crystal to have a phase matching temperature as high as practically possible. Alex Skliar [30] suggests that design temperatures in excess of 180 °C are impractical, but a design temperature of 170 ± 10°C is feasible; a future experiment can and should employ such a crystal to determine the utility of such an approach.

4.3 Final Design

The final design of my system closely follows the schematic laid out in section 1.5, with a picture thereof shown in figure 4.4.

The pumping lasers were aligned on pinholes, one of which is out of frame, to ensure that they both entered with the same mode vector: both were approximately 1.5 m away from the interferometer along the beam bath, with sufficient mirrors in place to align them precisely. At the edge of the frame is visible the QWP, mounted on a rotating platform mount, just behind it is the HWP to set the pump polarization. The pump then passes through a 200 mm focal length lens, mounted on a 60 mm square translation stage to fine-tune the position of the focus. The pump beam then passes through the back of the dichroic mirror and enters the interferometer loop, travelling in both directions. The HWP inside the loop is mounted cantilevered off of the right hand mirror's post, due to lack of space.

The large cylinder at bottom centre of frame is the oven for the PPKTP crystal, mounted via a homemade bracket to a tip-tilt stage and a 40 mm XY stage. The two outputs are coupled, via a polarization analyser and the long-pass filters, into fibre using five-axis fibre couplers and a 10X microscope objective. In the background can be seen fibre optics coiled on the optical bench; it should be noted that they are black-patched to reduce the amount of light captured into fibre from the environment.

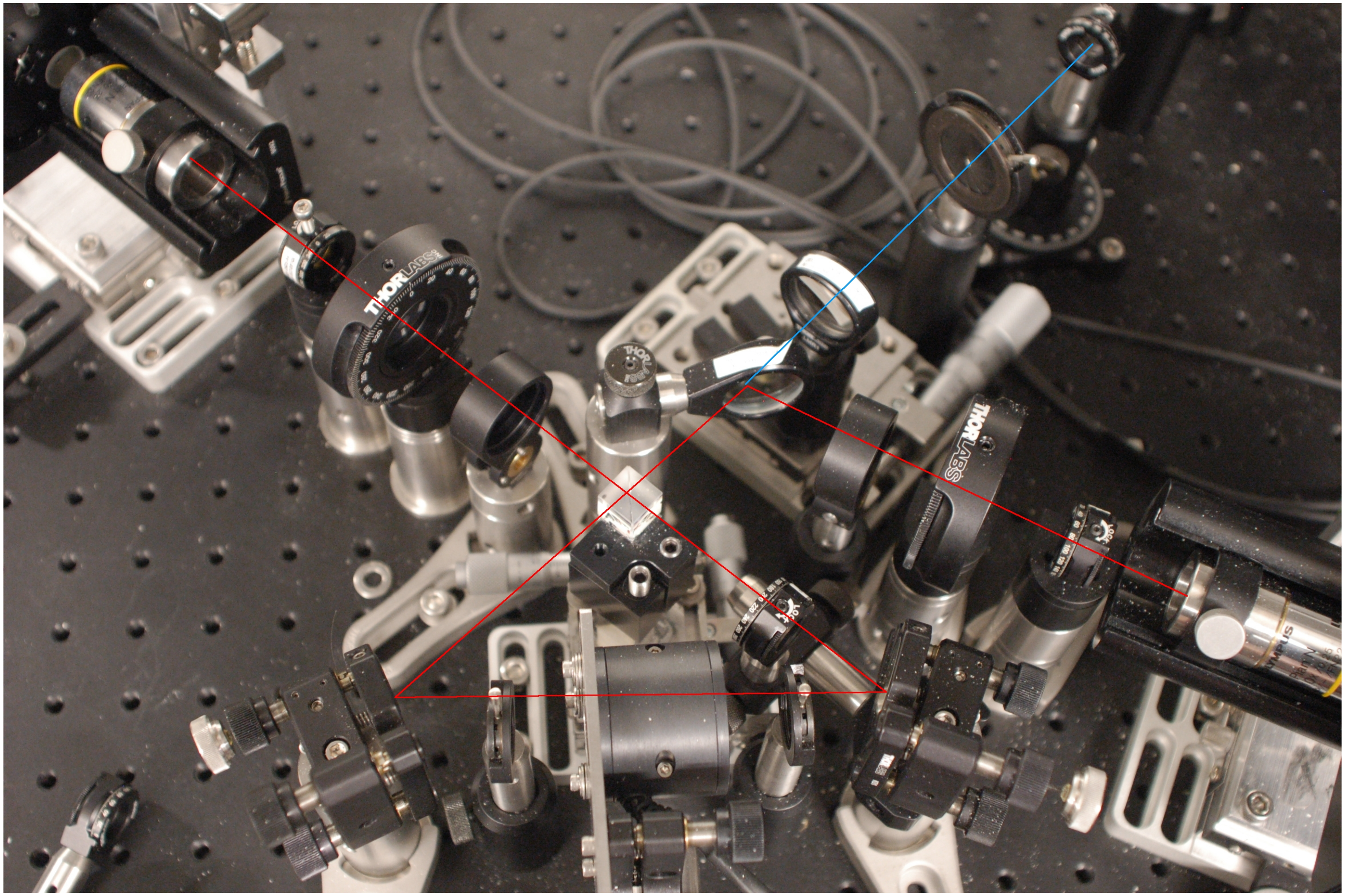

Figure 4.4: A picture of the experiment, as used for the results presented in this thesis. The triangle at the bottom of frame is the Sagnac loop, with the pump beam (blue line) entering from the top right. The left output of the interferometer is the signal channel, while the right hand one is the idler channel. Photograph courtesy Jen S. Fung

Chapter 5

Experimental Results

In this chapter I will present the results of my experiments with discussion accompanying the various data. The first portion of the chapter will cover the preliminary and interim results taken over the course of the experiments, and the latter portion will present the final results speaking directly to the goals of the experiment.

5.1 Preliminary Results

Before performing state tomography on the photon pairs produced in my experiment, various preliminary measurements were taken.

5.1.1 Stability

One desired feature of a photon source is stability over long periods of time. Fortunately, this is relatively simple to measure, if not to improve; doing so at least allows one to examine sources of noise. Figure 5.1 shows data taken over three days to examine the long-term stability of my source, which proved to be quite stable, only losing half of its coincidences over three days, or only .04 dB/hour. However, as shown in figure 5.2 there were several noise sources in the system: pink $(1/f)$ noise, as expected; daily cycle noise, which is not readily apparent in the Fourier transform but more obvious on the time-domain plot; and noise between 40 to 60 minutes in period, which is quite obvious on the time domain plot from minutes 1200 to 2500 and is almost certainly thermal fluctuations of the experimental apparatus due to the HVAC system.

Another experiment was done to determine the temperature sensitivity over a long period of time: as I had to heat the crystal to repair some grey tracking, I used the opportunity to measure the coupling as a function of temperature and time. Figure 5.3 shows curves for the signal and idler channel, and coincidences therebetween as the crystal was heated to 180°C at 10°C per hour, held there for four hours, and then cooled to room temperature at 10°C/hour. The system was aligned before the experiment began at 30°C nominal, and pumped with the Ti:Sapphire laser at approximately 10 mW.

As the temperature increased both channels' count rates decreased, recovering somewhat as the temperature was brought back down: this is not unexpected. The startling feature about figure 5.3 is the very large peak on the signal channel near 80°C on both

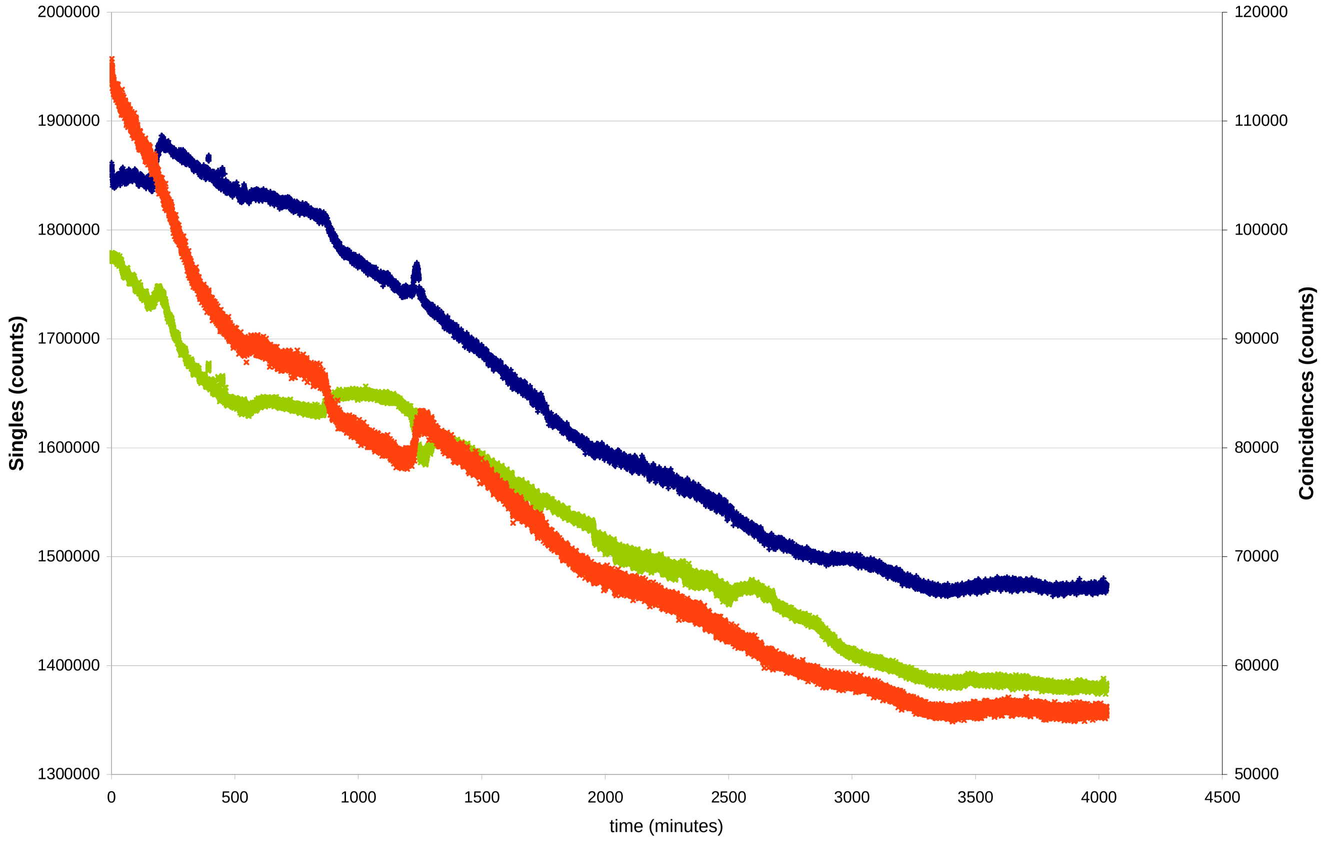

Figure 5.1: Singles and coincidences as a function of time over three days. Blue dots are signal counts and lime are idler counts, plotted on the left axis. Orange are coincidences, plotted on the right axis. Time intervals are 20 seconds, and the system was pumped with the Ti:Sapphire laser at approximately 10 mW.
Conditional coupling efficiency declined by a factor of 2 over 3 days, quite good given that the fibre couplers are aligned to 10 μm. However, there is noise at a period of 40-60 minutes (see figure 5.2) .

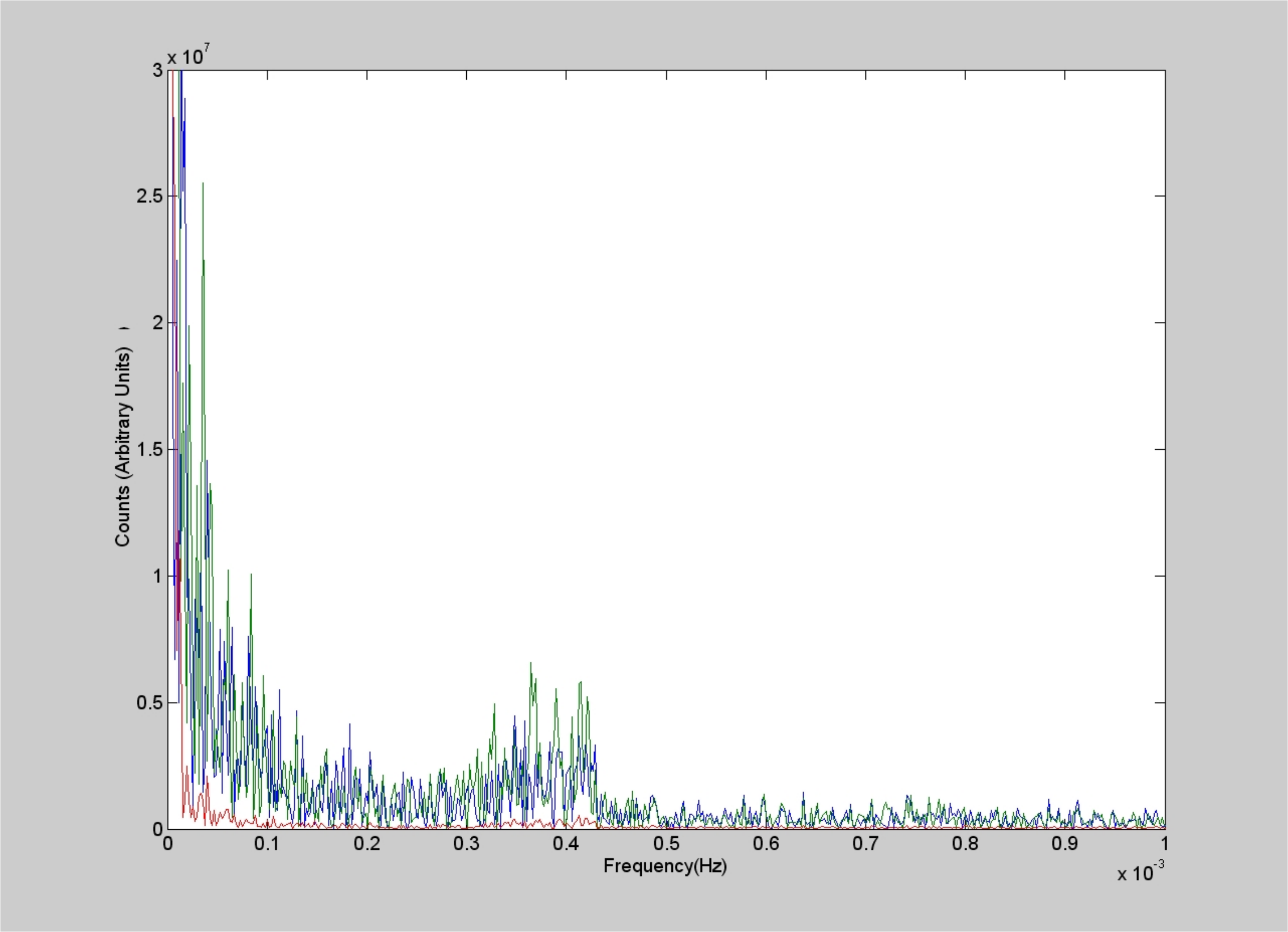

Figure 5.2: Fourier transform of the data in figure 5.1. The data follows the expected $1/f$ (pink) noise shape, with the exception of a noisy region at a period of 40-60 minutes due likely to the HVAC causing thermal fluctuations of some experimental components. The most likely component to be strongly coupled to the temperature is the fibre optic's tip positioning relative to its coupling objective.

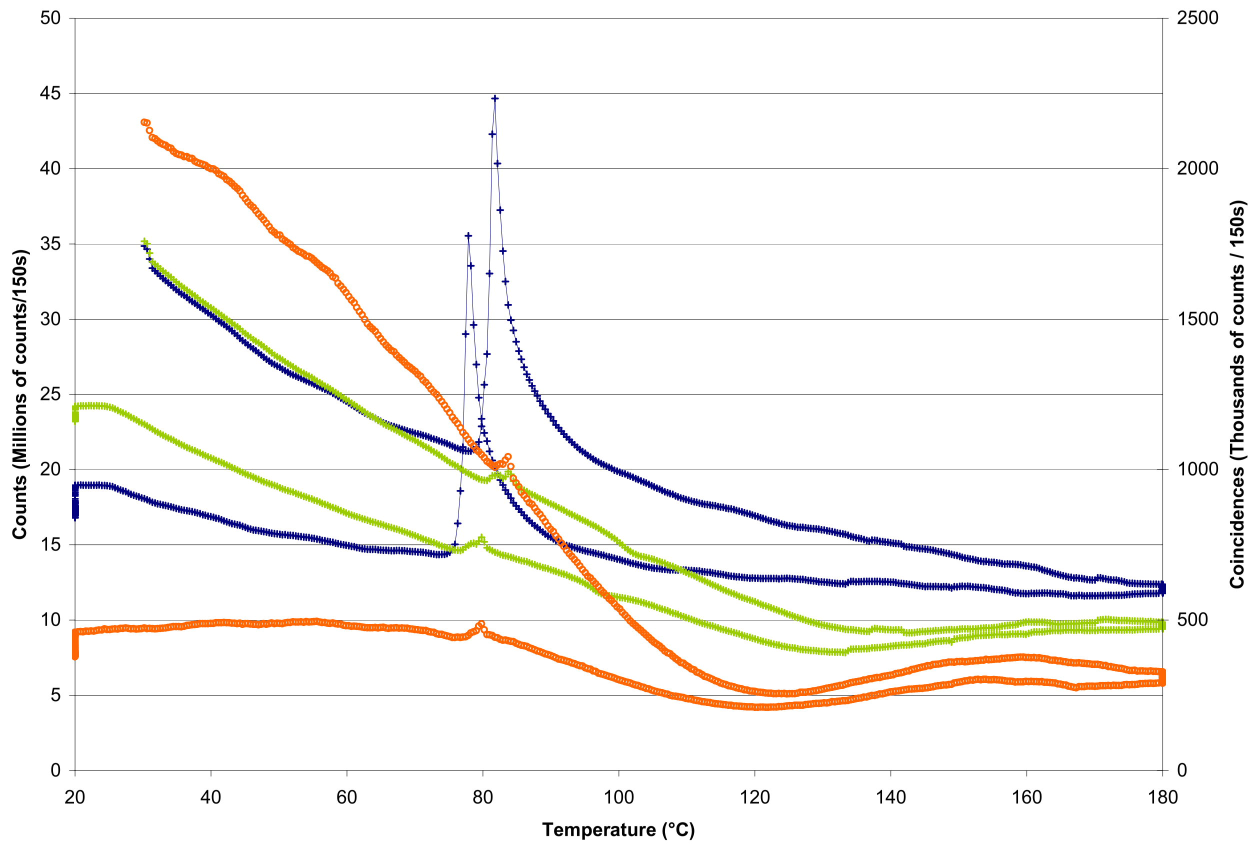

Figure 5.3: Single and coincidences as a function of temperature. Data taken over 42 hours, each point is 150 seconds. Blue, green and orange points are signal, idler, and coincidences respectively, with coincidences plotted on the right ordinate; the upper curves are temperatures increasing with time, the lower curve temperatures decreasing with time after holding at 180°C for 4 hours. Temperatures are interpolated from the setpoints on a PID temperature controller: they should be treated as having significant systematic error, as shown by the large peak on the signal channel, which should be at the same temperature both increasing and decreasing. The large peak near 80°C is type I SPDC.

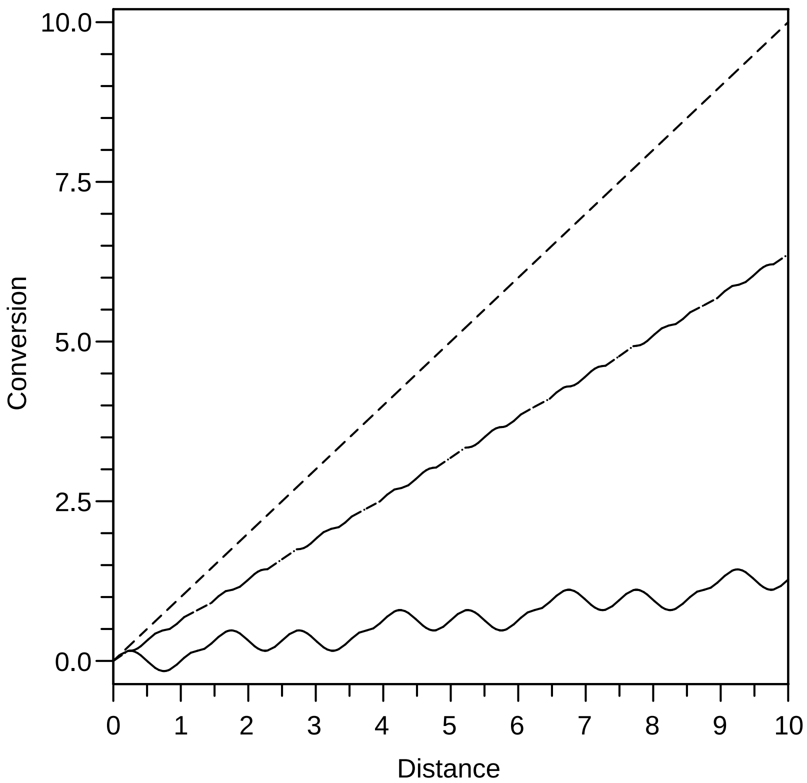

Figure 5.4: A plot showing the growth of perfectly phase matched (dashes), first order quasiphasematched (dots) and fifth order quasiphasematched (solid line) SPDC as a function of length in the crystal. Note that in all cases down conversion grows linearly with propagation distance up to local oscillations. The first and fifth order curves are set to have the same phase mismatch.

the increasing and decreasing temperature tracks: later investigations showed it to peak at 81°C.

After some experiments and calculations were performed, the conclusion was made that this is type-I SPDC, quasiphasematched at fifth order, that is, the quasiphasematching period for type-I SPDC in PPKTP is about 2 μm: as 2 divides 10, the poling period used, SPDC does proceed, albeit one-fifth as fast as if it were phase matched at first order, as shown in figure 5.4. As the $\chi^{(2)}$ component for type-I processes is much higher than that for type-II processes in KTP, the large peak is explained, as is its shape. Note that because it is a type I process that the peak is is quite narrow, and the sharp onset as temperature increases is also expected as below the degeneracy point there is no quasiphasematching solution, while the degenerate type-I is the most efficient, both in generation and translation through the system.

5.1.2 Losses

One important parameter to explore when examining experimental results is the level of loss in the system: this is especially important in determining the amount of overlap between the modes coupled into two fibres.

Optical losses in my setup are due primarily to reflections off of various optical components, as shown in table 5.1, plus the losses in the detectors: they are about 40% efficient

Item	Loss (dB)	Number	Net (dB)
Filter glass (3 mm)	0.087	2	0.174
Uncoated glass/air interface	0.117	6	0.702
PBS	0.080	1	0.080
Linear Polarizer (LPVIS050)	1.502	1	1.502
Dichroic mirror	0.110	0/1	0.110
Si SPADs (Perkin and Elmer)	3.98	1	3.98
Total	.		6.44

Table 5.1: The elements causing loss in my setup, measured individually. The uncoated glass/air interfaces are from two pieces of filter glass and two ends of a fibre optic. The total loss of 6.44 dB is equivalent to a transmission of 23%.

at 810 nm. Therefore, a maximum conditional coupling of 23% can be expected.

5.1.3 Fluorescence

The primary source of noise in the system was fluorescence the PPKTP crystal, predominantly from grey tracks (see 4.2.3). A measurement was made of the amount of fluorescence by taking two measurements of coincidence rates when the zero offset what set to exactly the pulse spacing, and set to some other non-zero time. As fluorescence is a slow process (on the timescale of the laser's repetition rate) it can be approximated as occurring at a constant rate, while SPDC, being fast, can be approximated as only occurring on the pulse interval.

For one measurement, made before I baked the crystal to take my final data runs (during which baking I took the data given in section 5.1.1), I found that the pulse-to-pulse reading gave 400 counts/s, while off the pulse spacing the reading was 188 counts/s on singles of 288 and 342 $\cdot 10^3$counts/s for the signal and idler channels. Then

$$(s_p i_f + i_p s_f + i_f s_f) \cdot 2 \text{ ns} = 188 s^{-1} \tag{5.1}$$

$$\frac{s_p i_p}{76 \text{ MHz}} + (s_p i_f + i_p s_f + i_f s_f) \cdot 2 \text{ ns} = 400 s^{-1} \tag{5.2}$$

$$\Rightarrow \frac{s_p i_p}{76 \text{ MHz}} = 212 s^{-1} \tag{5.3}$$

where s and i are the count rates on the signal and idler channels, and subscripts p and f refer to SPDC and fluorescence light respectively. Unfortunately, this is an under-complete system, in order to solve it I made the approximation that the ratio of SPDC and fluorescent light was equal in both channels. Given that assumption, I find that in this measurement the singles on the idler channel were 70% SPDC photons: that is, fluorescence makes a significant but not overwhelming contribution to the received signal.

5.1.4 Spectroscopy

Due to the large number of parameters involved in the production of PPKTP crystals, the phase matching temperature for degenerate SPDC is specified only within a 20 °C window. As we are pumping with several different lasers, one of which is tunable, spectroscopy was performed on the system to determine an optimal temperature: ideally that of degenerate SPDC.

Our crystals were designed for an operating temperature of 50 ± 10 °C at 405 nm; unfortunately, our laser diode at a nominal 405 nm lases at 404.2 ± 0.1 nm. This would not be a problem, except that lower wavelength pump lasers require lower temperatures to phase match degenerately, and in this case this temperature is below room temperature. The temperature control is strictly a heater, and thus for our CW experiments all of the SPDC photons were produced off-degeneracy. Figures 5.5 and 5.6 show spectrographs of the signal and idler channels, respectively, under CW excitation. The overlap between the two paths is at least 97% and the splitting between signal and idler is 25.8 ± 0.1 nm, with photon full bandwidths of 0.5 nm. Ideally, the splitting between signal and idler would be 0, so that all the optics operate at or near their design wavelength of 810 nm, but the crystal cannot be cooled below 28°C. Tuning the temperature changes the splitting between the peaks at 4.1 ± 0.2°C/nm in the regime studied, while extrapolating this gives a degenerate phase matching temperature of -80 ± 3°C, though this uncertainty certainly underestimates the error in the extrapolation due to nonlinearities and the usual risks in extrapolation.

Figure 5.7 shows a spectrograph of the source under pulsed excitation: the left hand peak is the signal at 798.8 nm with a bandwidth of 2.3 nm, while the right hand peak is stray Ti:Sapphire laser light, providing a reference wavelength and showing the broadening effect of SPDC, recalling that the laser is frequency doubled and then halved.

5.2 Final Results

5.2.1 Continuous-Wave Source

To provide context for the results in the next section, I must first show the performance of my system under conditions comparable to those reported in the literature by pumping it with a continuous-wave laser. Unfortunately, as documented above, it was not possible to set my crystal's temperature so as to achieve degenerate SPDC, degrading the performance of the optics.

Figure 5.8 shows a tomograph of the system in CW configuration ideally creating the triplet state $|HV\rangle + |VH\rangle$: the fidelity to this state is $.9726 \pm 0.0005$. This state had a tangle of $0.9097^{+0.0017}_{-0.0016}$.

The non-equality of the $|HV\rangle$ and $|VH\rangle$ components of the density matrix can be attributed to alignment error or experimental drift during the course of tomography: this should be correctable before my defence, at which updated data will be presented.

The brightness of this source was 600 pairs/s/mW detected, or, given the 0.5 nm bandwidth of the photons 1200 pairs/s/mW/nm, a figure much worse than that reported in Fedrizzi *et al.* [5], who reports for a 15 mm crystal a brightness of 65000 pairs/s/mW. A large part of the difference, however, can be attributed to differences in conditional coupling: they have a coupling rate of 28.5% as opposed to my value in this case of 5.7% (averaged over all paths). The conditional coupling affects the brightness quadratically, so a factor of 25 enters. Furthermore, my pump is attenuated on the insertion dichroic mirror by 18%, and the polarizing beamsplitter is quite poor at the pump wavelength. The remaining difference must be attributed to the misoptimization of my focal parameters.

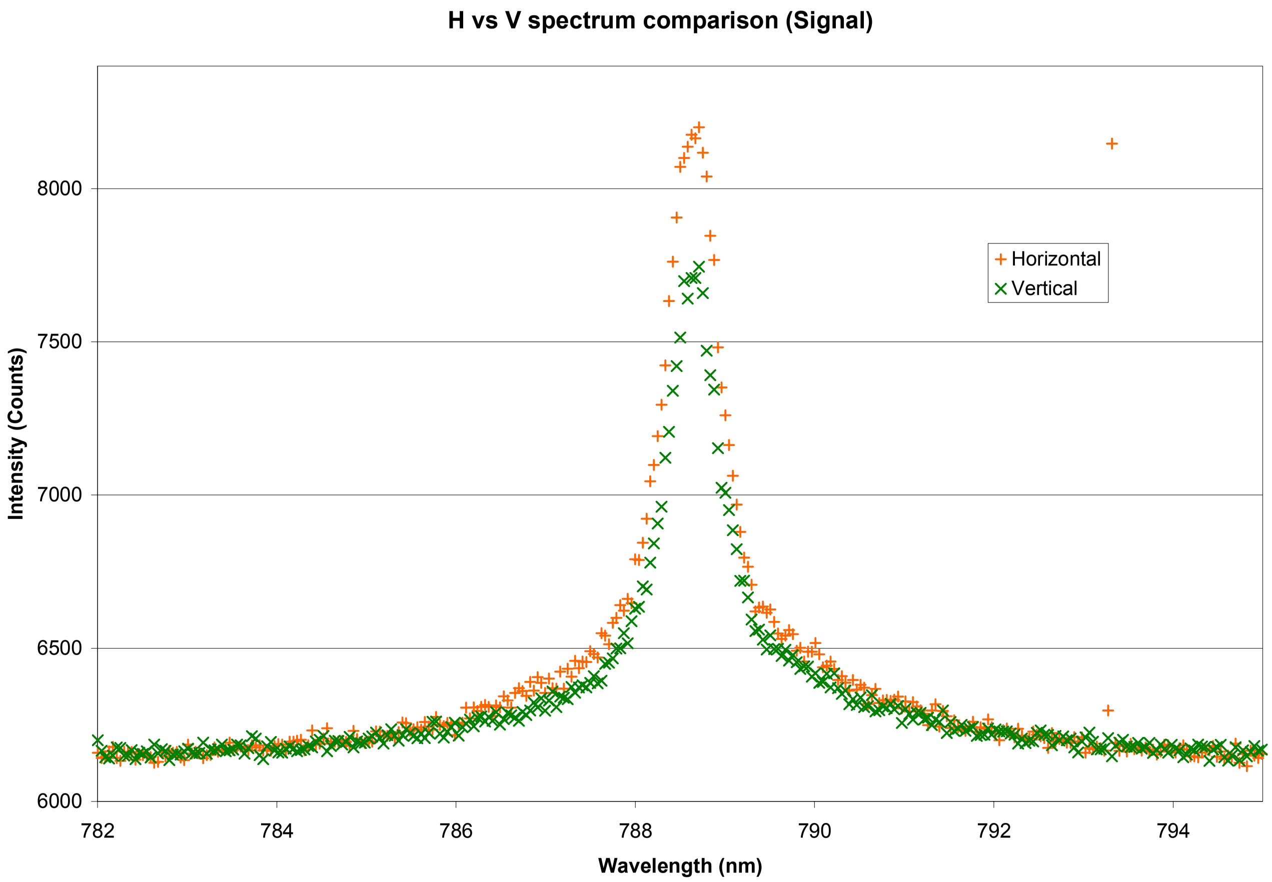

Figure 5.5: A spectrograph of the signal channel of my Sagnac source under CW excitation at 404.2 ± 0.2 nm. × are vertically polarized photons, while + are horizontally polarized. The crystal was held at 78 °C. Collection time was 20 minutes; the background is primarily instrumental: no background subtraction was done. The difference in the height of the peaks is tuning and alignment. The numerical overlap between the two peaks is approximately 97%.

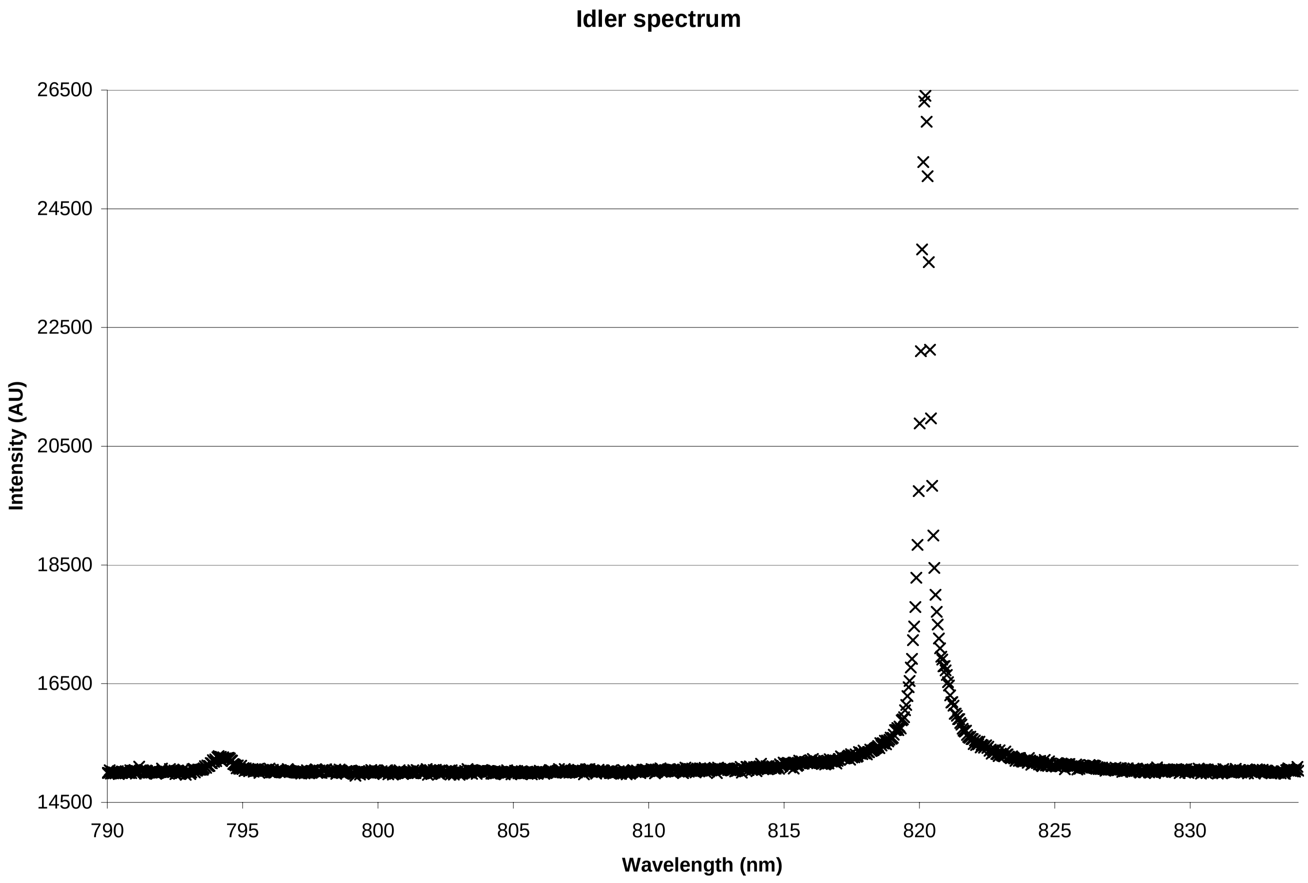

Figure 5.6: A spectrograph of the idler channel, circularly polarized, under CW excitation at 404.2 ± 0.2 nm. Collection time was 10 minutes and the crystal temperature was the lowest at which my oven was stable: 28°C; all experiments using this laser were performed at this temperature. The large peak at 820.2 ± 0.3 nm is the desired idler light, while the much smaller peak at 794.4 ± 0.3 nm is light received at this detector in error, having excited the wrong port of the Sagnac PBS due either to the HWP or the PBS performing nonideally.

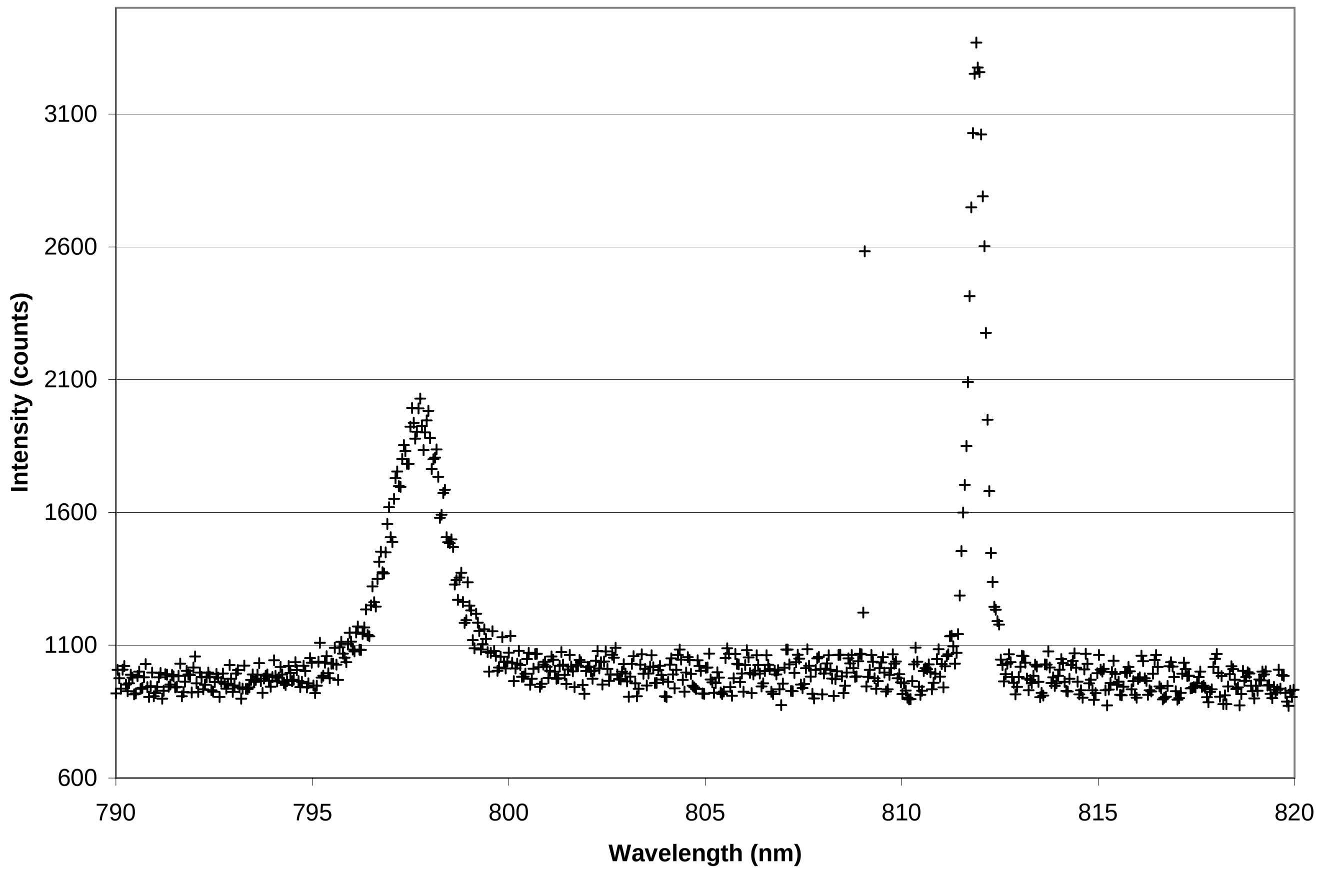

Figure 5.7: A spectrograph of the signal channel, horizontally polarized, under picosecond pulsed Ti:Sapph excitation. The left peak is the signal light at 798.8 nm with a bandwidth of 2.3 nm. (no error estimates yet.) The right peak is laser light entering the spectrometer from ambient: none or very little of it is being coupled at the fibre. It is tuned to 812 nm in this graph, though this is not where the system was operated

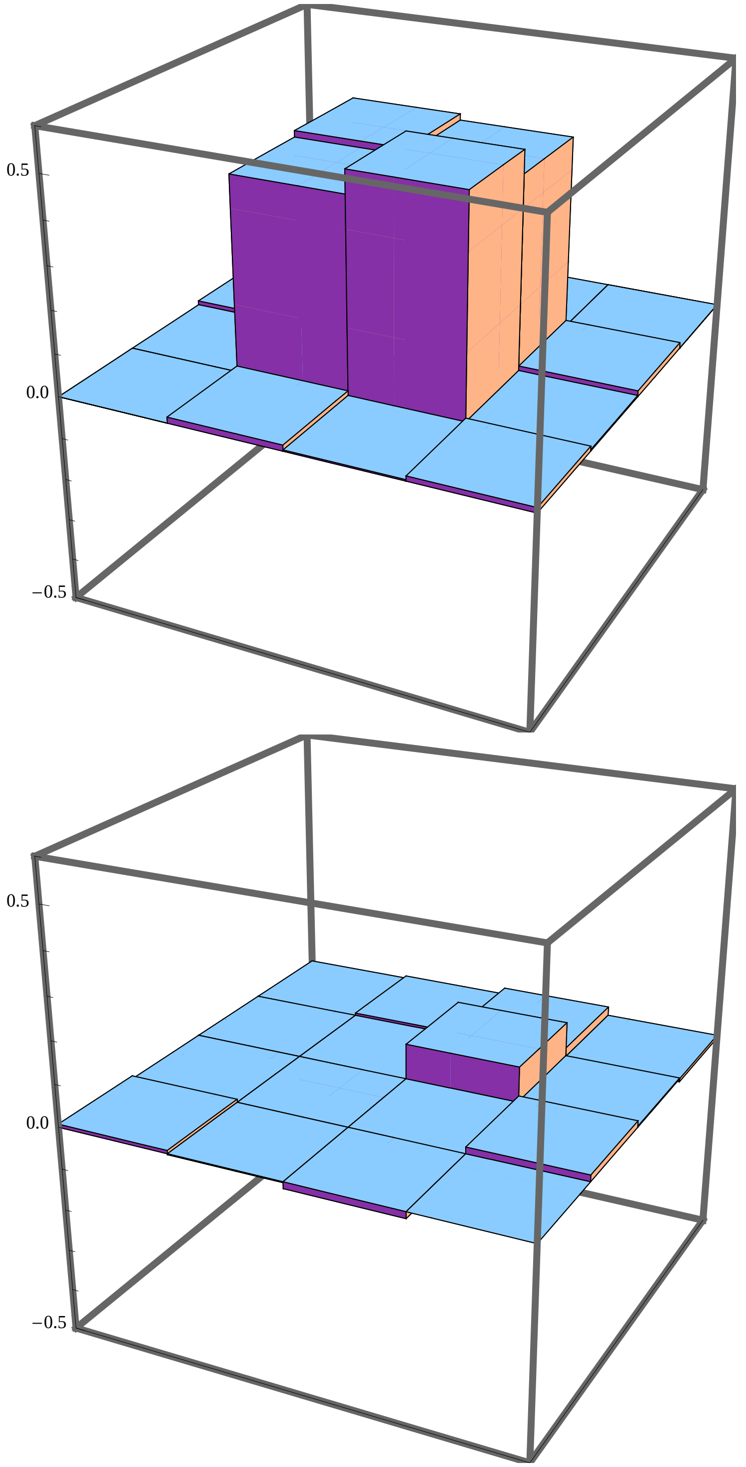

Figure 5.8: A tomograph of the quantum state output by my source pumped by a CW laser at 404.2±0.2 nm with a power of 30mW. The upper plot is the real component, while the lower plot is the imaginary component. The far corner of the plot is the state $|00\rangle \equiv |HH\rangle$, while the near corner is the state $|11\rangle \equiv |VV\rangle$. Ideally, the ρ_{11}, ρ_{12}, ρ_{21}, and ρ_{22} components would be 1/2, while the remainder of the elements would be zero. This is the triplet state $|01\rangle + |10\rangle$. Each measurement was taken for 10 s

5.2.2 Pulsed Source

Performance of my system when driven with a pulsed laser was comparable to that under the CW laser. Driven with 2 ps pulses at 810 nm at 76 MHz, with an average power incident upon the crystal of 12.4 mW, the system performed per expectations. A tomograph of the system is shown in figure 5.9. The system performed as expected, with a fidelity to the $|\psi^{+}\rangle$ state of 0.9798 ± 0.0004; the mismatch largely lies in an overabundance of $|HV\rangle$ photons, which should be correctable. New data will be presented at the defence of this thesis. The tangle of this state is $0.928 \pm .0015$, very similar to the CW result, which is itself surprising considering accidental events are much more likely in a pulsed configuration due to limited excitation times and higher fluorescence. The interference visibility in the $\{|0\rangle, |1\rangle\}$, $|\pm\rangle$, and $|\pm i\rangle$ bases was 96.8%, 92.3% and 90.5% respectively.

This source had a brightness of 597 ± 5 pairs/s/mW, or, dividing through by the 1.8 ± 0.1 nm bandwidth of the signal a spectral brightness of 330 ± 20 pairs/s/mW/nm. The number most comparable to the CW source above is the brightness, which is within error of the same value: no efficiency is lost changing from a CW to a pulsed source. The other figure which it is important to compare to is the performance of other photon pair sources pumped with ultrafast lasers: one such source[31] had an entanglement visibility of 95% and a brightness of 5 pairs/s/mW, the latter much worse than I am reporting here.

Note that while the grey-tracking reported earlier is a significant contribution to the total singles counts they are sufficiently low in number not to overwhelm the parametric down-converted photons detected. The fluorescence photons do reduce the entanglement quality, as they represent about 4% of all of the coincidences even at the low power being used in this experiment, and moreover complicate alignment. However, they do not present a fatal obstacle to the operation of the source.

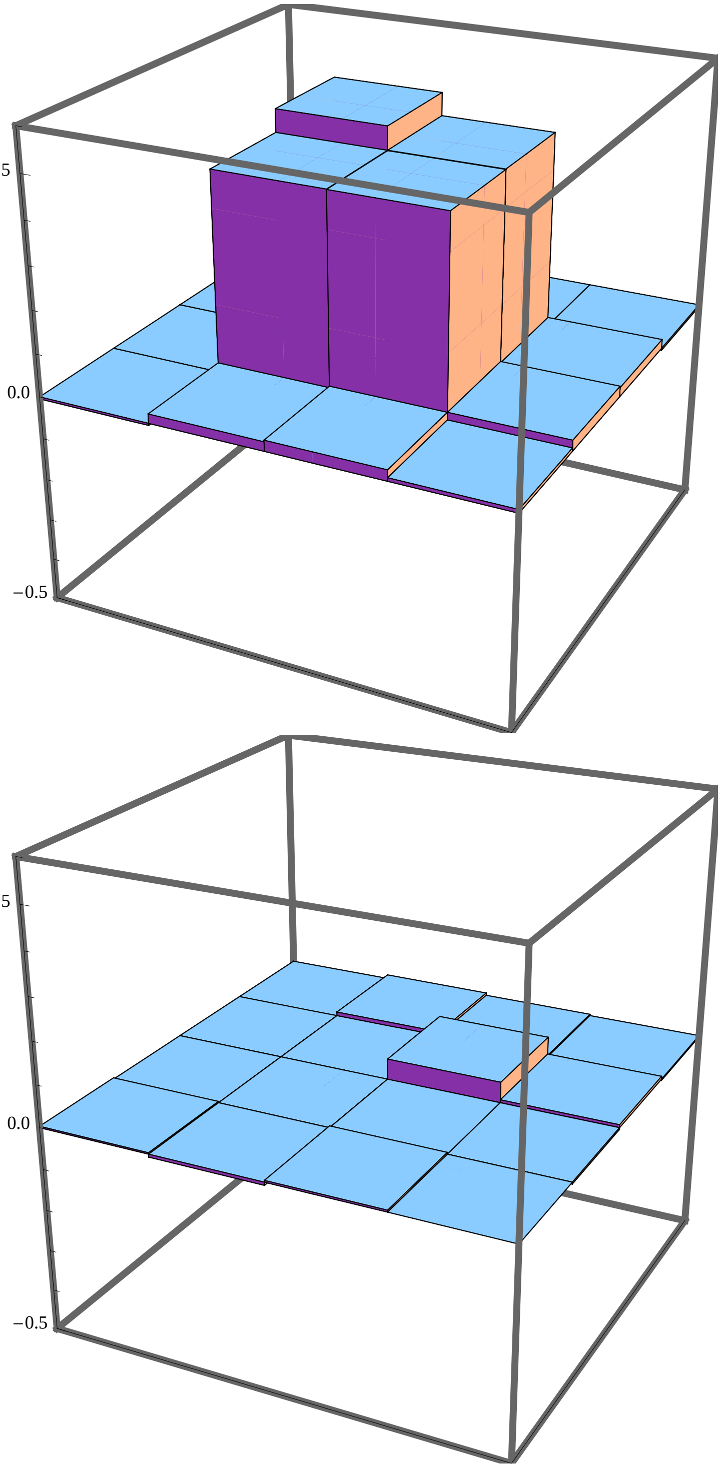

Figure 5.9: A state tomograph of the source's output under excitation from a Ti:Sapph laser with 2 ps pulses at 810 nm at a repetition rate of 76 MHz. Orientation as the previous tomograph. This tomograph again shows a slight mismatch in the amount of $|HV\rangle$ and $|VH\rangle$ present: this is correctable and should be improved before this thesis is defended. The fidelity to the $|\psi^+\rangle$ state is 0.9798 ± 0.0004, and the tangle is 0.928 ± 0.0015. Each measurement was taken for 20 s.

Chapter 6

Conclusions and Future Developments

In this thesis, I have shown two important things: that a Sagnac-type photon pair source is viable when pumped with an ultrafast laser, and that a dual-interferometer design is unfeasible.

First and most importantly, I have demonstrated the feasibility of a Sagnac source for photon pair generation using an ultrafast laser. Hopefully this will be extendable to a four-fold experiment in the future in one of two ways: either by increasing the pumping rate to generate four-fold events in a single Sagnac system; or by using two such sources for experiments such as entanglement swapping. A plan is in place for the latter to be attempted using my source as a template in the near future.

Secondly, I have demonstrated a negative result: that our proposed "dual Sagnac" design was suboptimal. Fraught with experimental difficulties, the design proved to be too experimentally unpleasant relative to the standard Sagnac design for little benefit.

The future holds several possibilities: as mentioned above, the next logical step in the proof of the viability of sources of this type for pulsed quantum optics is to demonstrate entanglement swapping or similar four-fold experiments. One possible scheme for generating four-fold events is to pump the system at two wavelengths, generating pairs at two different sets of down-conversion wavelengths that can be separated dichroically.

Another is to attempt to run my source with femtosecond excitation; attempts to do so in Vienna failed, but they had not previously used picosecond excitation, nor was their source designed for pulsed excitation. I am not certain that this will succeed at all, let alone in a useful fashion, but it is worth trying, especially as my source is already being pumped by a Ti:Sapphire laser that can be readily converted to femtosecond operation.

A third possibility, which seems reasonably promising, is to substitute a weak PP-KTP waveguide for the free-space crystal currently in use. This should increase the pair generation rate without requiring the very precise and highly focused coupling of a strong waveguide. With luck, the focusing optics could remain outside the Sagnac loop if it were made sufficiently small.

The last possible extension, and one which involves knowledge that I do not have, is to try and find a less easily damaged crystal for use in these sources. As mentioned in section 4.2.3, one possible solution is to simply elevate the operating temperature of the crystal: this is the most obvious and easiest thing to try. The other possibility is to substitute a different crystal, perferably quasiphasematched for collinear SPDC: an attempt by Xing Xingxing and coworkers [32][7] to use BBO cut at an angle in a similar source was abandoned due to experimental difficulty.

Bibliography

[1] T. Kim, M. Fiorentino, and F. N. C. Wong. Phase-stable source of polarization-entangled photons using a polarization Sagnac interferometer. *Phys. Rev. A*, 73:012316, 2006. 1, 2, 12, 15, 17

[2] G. Sagnac. L'éther lumineux démontré par l'effet du vent relatif d'éther dans un interféromètre en rotation uniforme. *Comptes Rendus*, 157:708–710, 1913. 1

[3] A. A. Michelson and H. G. Gale. The effect of the Earth's rotation on the velocity of light. *The Astrophysical Journal*, 61:140–145, 1925. 2

[4] O. Kuzucu and F. N. C. Wong. A pulsed Sagnac source of narrowband polarization-entangled photons. *Phys. Rev. A*, 77:032314, 2008. arXiv:0710.5390 [quant-ph]. 2, 28

[5] A. Fedrizzi, T. Herbst, A. Poppe, T. Jennewein, and A. Zeilinger. A wavelength tunable fiber-coupled source of narrowband entangled photons. *Opt. Express*, 15:15377–15386, 2007. 2, 18, 29, 30, 44

[6] D. Biggerstaff, M. Pereira de Almeida, M. Barbieri, and A. White. A sagnac source. 2006. 2

[7] F. Wolfgramm, X. Xing, A. Cerè, A. Predojević, A. M. Steinberg, and M. W. Mitchell. Bright filter-free source of indistinguishable photon pairs. *Opt. Express*, 16:18145–18151, 2008. arXiv:0806.4090v2 [quant-ph]. 2, 52

[8] R. Jozsa. Fidelity for mixed quantum states. *Journal of Modern Optics*, 41(12):2315–2324, December 1994. 4

[9] R. Horodecki, P. Horodecki, M. Horodecki, and K. Horodecki. Quantum entanglement. *Rev. Mod. Phys*, In process, 2007. arXiv:quant-ph/0702225v2. 5

[10] V. Coffman, J. Kundu, and W. K. Wootters. Distributed entanglement. *Phys. Rev. A*, 61(5):052306, Apr 2000. 5

[11] W. K. Wootters. Entanglement of formation of an arbitrary state of two qubits. *Phys. Rev. Lett.*, 80(10):2245–2248, Mar 1998. 6

[12] Nathan Langford. *Encoding, manipulating and measuring quantum information in optics.* PhD thesis, University of Queensland, July 2007. http://quantum.info/publications/langford_phd-final-070606-UQprint.pdf. 6, 7, 9

[13] D. F. V. James, P. G. Kwiat, W. J. Munro, and A. G. White. On the measurement of qubits. *Phys. Rev. A*, 64:052312, 2001. arXiv:quant-ph/0103121v1. 8

[14] M. Żukowski. Lecture notes. These appear not to be available on the web, but are in reasonably wide circulation. 10

[15] M.M. Fejer, G.A. Magel, D.H. Jundt, and R.L. Byer. Quasi-phase-matched second harmonic generation: tuning and tolerances. *Quantum Electronics, IEEE Journal of*, 28(11):2631–2654, Nov 1992. 11

[16] A. Ling, A. Lamas-Linares, and C. Kurtsiefer. Absolute emission rates of spontaneous parametric down conversion into transverse Gaussian modes. *Phys. Rev. A*, 77:043834, 2008. arXiv:0801.2220v2 [quant-ph]. 12, 29

[17] T. E. Keiss, Y. H. Shih, A. V. Sergienko, and C. O. Alley. Einstein-Podolsky-Rosen-Bohm experiment using pairs of light quanta produced by type-II parametric down-conversion. *Phys. Rev. Lett.*, 71(24):3893–3897, December 1993. 14

[18] C. E. Kuklewicz, M. Fiorentino, G. Messin, F. N.C . Wong, and J. H. Shapiro. High-flux source of polarization-entangled photons from a periodically poled $KTiOPO_4$ parametric down-converter. *Phys. Rev. A*, 69(1):013807, Jan 2004. 14

[19] P.G. Kwiat, K. Mattle, H. Weinfurter, A. Zeilinger, A.V. Sergienko, and Y. Shih. New high-intensity source of polarization-entangled photon pairs. *Phys. Rev. Lett.*, 75(24):4337–4342, 1995. 15

[20] G. Weihs, T. Jennewein, C. Simon, H. Weinfurter, and A. Zeilinger. Violation of Bell's inequality under strict Einstein locality conditions. *Phys. Rev. Lett.*, 81(24):5039–5043, 1998. 15

[21] T. Jennewein, C. Simon, G. Weihs, H. Weinfurter, and A. Zeilinger. Quantum cryptography with entangled photons. *Phys. Rev. Lett.*, 84(20):4729–4732, 2000. 15

[22] C. Erven, C. Couteau, R. Laflamme, and G. Weihs. Entangled quantum key distribution over two free-space optical links. *Opt. Express*, 16:16840–16853, 2008. 15

[23] M. Fiorentino, G. Messin, C. E. Kuklewicz, F. N. C. Wong, and J. H. Shapiro. Generation of ultrabright tunable polarization entanglement without spatial, spectral, or temporal constraints. *Phys. Rev. A*, 69(4):041801, Apr 2004. 15, 16

[24] J. H. Shapiro and N. C. Wong. An ultrabright narrowband source of polarization-entangled photon pairs. *Journal of Optics B: Quantum and Semiclassical Optics*, 2:L1–L4, February 2000. 21

[25] J.P. Fève, B. Boulanger, G. Marnier, and H. Albrecht. Repitition rate dependence of grey-tracking in $KTiOPO_4$ during second harmonic generation at 532nm. *Applied Physics Letters*, 70(3):277–279, January 1994. 21, 35

[26] C. Erven. On free space quantum key distribution and its implementation with a polarization-entangled parametric down conversion source. Master's thesis, University of Waterloo, 2007. 25

[27] B. Boulanger, I. Rousseau, J.P. Feve, M. Maglione, B. Menaert, and G. Marnier. Optical studies of laser-induced gray-tracking in KTP. *Quantum Electronics, IEEE Journal of*, 35(3):281–286, Mar 1999. 28, 36

[28] A. Smith. Sandia National Labs Optics (SNLO) v40. Computer programme. 29

[29] D. Ljunggren and M. Tenger. Optimal focusing for maximal collection of entangled narrow-band photon pairs into single-mode fibers. *Phys. Rev. A*, 72:062301, 2005. 29

[30] A. Skliar. Private communication via e-mail, 25 Nov. 2007. Applications engineer for Raicol Crystals, Ltd. 36

[31] R. Kaltenbaek. *Entanglement Swapping and Quantum Interference with Intependent Sources.* PhD thesis, Universität Wien, February 2008. 49

[32] Xing X. Presentation at Quantum North workshop and private communication. 52